EVALUATION OF MOLYBDENUM AS AN ELECTRODE MATERIAL FOR AFFINITY BASED URINE DIPSTICK BIOSENSING

by

Vikramshankar Kamakoti

APPROVED BY SUPERVISORY COMMITTEE:

Dr. Shalini Prasad, Chair

Dr. Hyun-Joo Nam

Dr. Anjan Panneer Selvam

Dr. Todd W. Polk

Dedicated to my family

EVALUATION OF MOLYBDENUM AS AN ELECTRODE MATERIAL FOR AFFINITY BASED URINE DIPSTICK BIOSENSING

by

VIKRAMSHANKAR KAMAKOTI, B.TECH, MS

DISSERTATION

Presented to the Faculty of

The University of Texas at Dallas

in Partial Fulfillment

of the Requirements

for the Degree of

DOCTOR OF PHILOSOPHY IN

BIOMEDICAL ENGINEERING

THE UNIVERSITY OF TEXAS AT DALLAS

August 2017

ACKNOWLEDGMENTS

I thank my advisor, Dr.Shalini Prasad for guiding me in my research throughout the PhD program. I thank Dr.Anjan Panneer Selvam for mentoring me during the PhD program. My sincere thanks to other committee members Dr. Polk and Dr. Nam for their acceptance to serve on my supervising committee in my PhD program. I thank you for the constructive criticism in my research. I express my sincere thanks to Dr. Rajeshwari Taruvai Kalyana Kumar and Dr. Nandhinee Radha Shanmugam for providing constructive criticism to my research work. I thank Dr. Vinay J. Nagaraj for his guidance in a collaborative research work. I would like to thank my friends Badrinath Jagannath, Ambalika Sanjeev Tanak, Ashlesha Bhide, David Kinnamon, Jonathan E. Craven and Dr. Rujuta Munje for their support and encouragement during my PhD program.

Finally I thank my parents and my elder sisters for their support throughout my education.

July 2017

EVALUATION OF MOLYBDENUM AS AN ELECTRODE MATERIAL FOR AFFINITY BASED URINE DIPSTICK BIOSENSING

Vikramshankar Kamakoti, PhD
The University of Texas at Dallas, 2017

Supervising Professor: Dr. Shalini Prasad

The work presented in this dissertation focuses on evaluation and characterization of molybdenum (Mo) as an electrode material for affinity based biosensing applications. The material properties of the electrode material dictate the performance of electrochemical biosensors. Mo demonstrates electrochemical properties upon its interaction with electrolytes. Here, we have evaluated the electrochemical properties of Mo for use in affinity based biosensors. Surface characterization of deposited Mo electrode helps us to evaluate the efficiency of fabrication process conditions.

The deposition profile of Mo on the flexible polyamide (PA) substrate was characterized through Scanning Electron Microscopy (SEM) and Atomic Force Microscopy (AFM) techniques. A label-free immunoassay was designed for detection of target biomolecules. A monolayer of crosslinker was formed on the Mo electrode surface. Thiol and carbodiimide crosslinker chemistries were evaluated with Mo electrode. The characterization of chemical affinity between Mo and crosslinker molecules is required to understand the effectiveness of crosslinker monolayer formation on the electrode surface. The affinity between electrode and crosslinker molecules were characterized through Fourier Transform Infrared Spectroscopy (FTIR), Fluorescence microscopy and X-ray photoelectron spectroscopy (XPS). The binding affinity between antibody and

crosslinker molecules was also characterized using FTIR technique. The form factor of the biosensor was modified as a dipstick to detect inflammatory biomarkers namely Interleukin (IL-6) and C-reactive protein (CRP). The effect of variable pH of the synthetic urine on the detection of CRP and Il-6 was evaluated using Electrochemical Impedance Spectroscopy (EIS) technique. The portability of the biosensor was demonstrated using customized electronics hardware assembly. The impedance response from the electronics hardware was compared against standard potentiostat systems.

TABLE OF CONTENTS

LIST OF FIGURES

LIST OF TABLES

CHAPTER 1

INTRODUCTION

Biosensors are standalone devices which provide analytical information on a target biomolecule.[1] The biosensor consists of three sub-systems namely the biological recognition element, transducer element and the signal processing element. The design of biosensors involves solving technical challenges in these three sub-systems and it involves multi-disciplinary knowledge in the fields of material science, biology and electrical engineering. The specificity of the biosensor is principally governed by the biological recognition element. Antibodies and Nucleic Acid probes are the most prominent recognition elements which have been evaluated in the design of biosensors. The binding event between the target biomolecules and the biological recognition element is captured by transducer element. There are various transduction methods (optical, electrochemical, piezoelectric etc.) which have been employed to convert the signal from the target analyte to the detector system. The signal processing element is critical for efficient readout of the measured signal. The rest of this chapter explains the significance of label-free biosensors and discusses the properties of Mo which are relevant for their evaluation in electrochemical biosensors. Chapter 2 discusses the fabrication of molybdenum electrodes and signal transduction principles. Chapter 3 describes the novelty of this work and relevance of this research towards designing affinity based biosensors. Chapter 4 describes the surface morphology analysis of Mo electrodes and explains its application for demonstrating of electrochemical biosensing. Chapter 5 explains the chemical interactions between Mo and crosslinker molecules towards the formation of crosslinker

monolayer. Chapter 6 explains the application of Mo for design of electrochemical dipstick biosensors for detection of inflammatory biomarkers in urine.

Labeled and label-free based biosensors are primary classifications of affinity based biosensors. Label-based biosensors involves the tagging of a label to the target analyte.[2] The quantitative measurement of the labels post the biomolecular binding is estimated to correspond to the target analyte's concentration. However, the variability in the analyte and label binding properties might lead to output readout errors. Label-free biosensors enable real-time monitoring of biomolecular binding which favor their use in point of care applications.

The point of care (PoC) biosensors are used for home or clinic based diagnostic systems for obtaining useful information regarding early disease diagnosis and prognosis. The advent of PoC biosensors has enabled quick access to healthcare in a resource challenged environment. These devices enable rapid diagnosis of target analytes and hence there is no requirement for sample transport to laboratories for analysis. Thus, the patient has the scope for knowing results of the testing instantly. This feature has greatly enabled in improving the quality of life of patients, and it also helps in saving causalities occurring from fatal diseases. The form factor of the PoC devices are significantly lower than the conventional laboratory diagnosis equipments.[3] The portable diagnostic devices do not generally require complex sample preparation techniques which facilitates their use in home based monitoring and diagnosis of the physiological condition. The sensor cartridges of PoC biosensors are generally disposable which greatly reduces the cleaning requirements of the instrumentation hardware. The output of these devices are designed for easy interpretation in a qualitative or quantitative way. Colorimetric biosensors are an example of qualitative biosensors wherein the output from the biomolecular binding is reflected as changes in

the color. The variability in the changes in the color gradient is one of the critical challenges of the colorimetric based biosensors. Electrical biosensors provide quantitative output in terms of voltage/current changes. They are classified as voltammetry, amperometric or impedance based biosensors. Impedance based biosensors are favored for ease with portability, ease of integration with external hardware, low cost and the ability to provide quantitative output results. The electrochemical properties of electrode material greatly influence the output signal response of the biosensor. Hence, it is favorable to evaluate elements which demonstrate favorable electrochemical properties. In this regard, the electrochemical properties demonstrated by Mo on its interaction with electrolyte support their evaluation as electrode material in affinity based electrochemical biosensors.

The objective of this work is to evaluate molybdenum (Mo) as an electrode material for affinity based electrochemical biosensing application. Flexible nanoporous polyamide (PA) membranes have been used as the sensor substrate.

Characteristics of molybdenum

Molybdenum (Mo) is a refractory metal belonging to the transition group of elements and demonstrates BCC crystalline structure.[4] It possess low wear resistance, good thermal and electrical conducting properties. It is also considered a favorable alloying element as it increases mechanical properties of the alloy.[5] A thin passive surface oxide is formed on the molybdenum surface which attributes to its high corrosion resistance. Molybdenum oxides find wide applications like electrocatalysis, lithium ion batteries, gas sensors, capacitors, fuel cells and other applications. The change in conductance of molybdenum oxide upon the adsorption/reaction is the basis to apply it for gas sensing applications. Mo possesses good electrical conductivity properties

and has been used as a bottom electrode material in bulk acoustic resonator applications.[6] Mo has been used as a gate electrode in thin film transistors.[7] Thicker electrical double layer has been observed for molybdenum electrode compared to Nickel and Platinum in the hydrogen production through water electrolysis in 1-butyl-3-methylimidazolium tetra fluoroborate (BMI.BF4) through Electrochemical Impedance Spectroscopy (EIS) technique.[8] Molybdenum exhibits multiple oxidation states from II to VI and hence it demonstrates rich binding chemistry which facilitates the formation of multiple compounds with varying stoichiometry. Another significant property of Mo is the phenomena of pseudocapacitance demonstrated by Mo.[5] The compounds of molybdenum have also been found applications in semiconductor industry. Transition metal dichalcogenides (TMDs) have been used as an electrocatalysts.[9] Molybdenum Disulphide (MoS_2) has many industrial and research applications. It has been used as a gate material in Field Effect Transistors (FET).[10] The earliest industry applications of MoS_2 include their use as extreme pressure lubricants.[11] It has been used a solid lubricant and has been used in combination with hydrophobic and hydrophilic media and has been used as a dry film lubricant. It is added as a thermoplastics as a nucleating agent as it enhances mechanical properties. It has also been used in high density batteries. Molybdate (sodium molybdate) has been used as smoke suppressants. The thermal expansion of Mo is comparable with that of Silicon and hence it has been used in semiconductor applications. Mo possess good corrosion resistance against acids and therefore used in autoclave liners, funnels etc. The catalytic effect of molybdenum carbide is utilized in the development of solar cells.[12] Molybdenum silicides have been used in the production of oxygen protecting films owing to their corrosion and oxidation resistance. Molybdenum chloride have

been used for the detection of molecular oxygen due to their favorable optical and physical properties.[13]

Suitability of Mo for biosensing applications

Mo demonstrates good electrical conducting properties. The favorable electrochemical properties of Mo and its oxides have been applied to their use as an electrode material in fuel cells. They are used as an anode material in Lithium ion batteries owing to their high energy storage capacity. There has been a growing interest in MoS_2 based biosensors for quantification of analytes.[14] The formation of passive surface oxide layer on molybdenum electrode surface is a critical challenge in the formation of monolayer of crosslinkers towards building affinity based biosensor. The choice of crosslinkers is restricted to the use of those crosslinker molecules which have affinity to bind to oxygen site of molybdenum surface. Mo forms oxide compounds with varied stoichiometry which is correlated with its oxidation state. The molybdenum trioxide (MoO_3) is the oxidation product of other oxide compounds and is commonly observed as α layered structures. MoO_3 can accommodate amine and alcohol functional groups which is favorable for the formation of a chemical conjugate with organic functional groups of the crosslinkers. Mo is also a constituent in many enzymes and its presence is ubiquitous in the environment. These enzymes exhibit chemical affinity towards organic functional groups during various biochemical reactions inside the human body.[15] Thus, the favorable properties demonstrated by Mo and its compounds support its evaluation as an electrode material for development of electrochemical biosensors.

Deposition of molybdenum thin films

Electron beam evaporation, DC and RF sputtering are the most commonly reported deposition methods for the development of Mo thin films. The optimization of process parameters is a critical step which govern the nature of the deposition profile and physical properties of thin films.[16] Many researches have evaluated the effect of process parameters by varying the deposition power, duration of deposition, method of deposition, presence of inert gases, presence of oxygen etc. The variation of these parameters might affect the conductive and material properties of the Mo thin films. The resistivity of the thin film is dependent on deposition power. In DC magnetron sputtering technique, higher deposition power yielded thin films with low electrical resistivity.[17] The adhesion of Mo thin films could also enhanced by increasing the deposition power.[18] It has been demonstrated that the Argon (Ar) pressure has a direct relation with electrical sheet resistance.[19] The nature of the thin film is dependent on the application for which the Mo thin film is being deposited. For Impedimetric biosensing applications, conductive thin films are desired as it enhances the conduction of current resulting from biomolecular binding. The characterization of deposition profile post fabrication is imperative in understanding the efficiency of the deposition technique and accordingly optimize the process parameters.

In this work, we have achieved planar deposition of Mo on flexible nanoporous polyamide substrate through electron beam evaporation technique. The rate of deposition was maintained constant for the deposition process and a thickness of 100 nm was achieved.

Electrochemical affinity based biosensing with Mo electrode

Affinity based biosensing of electrochemical biosensors is dependent on signal transduction resulting from biomolecular binding. Metal electrodes have been used for affinity based electrochemical biosensors due to its favorable electrical conducting properties. Gold has been preferred choice of electrode material in many affinity based electrochemical biosensors due to inert nature and favorable binding affinity to crosslinkers.[20] There has been a growing research in other transition group elements which demonstrate excellent electrochemical properties. Molybdenum demonstrates excellent electrochemical properties due to varied oxidation states exhibited by Mo from 2 to 6. Thus, it holds promise to be used as an electrochemical biosensing electrode favoring charge transfer properties of Mo.

CHAPTER 2

MATERIALS AND METHODS

Introduction

The design process of a biosensor involves the integration of various building block elements. The successful integration of these building block elements is required for getting reliable signal response. The various building elements of the sensor are the sensor substrate, electrode material deposition process, cross-linker characterization and testing the biomolecular binding through a transduction phenomenon. Efficient optimization at each step is imperative for achieving reliable signal response resulting from biomolecular binding. The following sections describe the individual elements of the biosensor design process.

Substrate material

The choice of the sensor substrate has been a major element defining the progress of biosensing technology. The emergence of flexible substrate for biosensing applications has facilitated the development of many disposable low cost biosensors.[21] Flexible substrates also favor mass fabrication of sensors through various batch fabrication techniques such as roll-to-roll manufacturing techniques.[22] Various materials have been evaluated as use as flexible substrate for biosensors such as Nylon, Polyethylene terephthalate (PET), polyamide etc.[23] Porous polyamide track etched membrane of porosity 200 nm has been used as a substrate for this work. The hydrophilic nature of polyamide substrate is advantageous for surface functionalization of biomolecules. The presence of nanoporous structures on sensor substrate also helps in charge

screening thereby minimizing non-specific biomolecule signal response.[24] The material characterization of electrode on the flexible polyamide substrate is discussed in Chapter 4.

Sensor fabrication

In this section, the various process steps followed for sensor fabrication have been described. The electrode pattern of the biosensor was made with AutoCAD software. The electrode pattern is transferred on to the sensor substrate with the use of transparent shadow masks. The shadow masks are aligned with the substrate and mounted on the chuck of the electron beam evaporator tool at UTD Cleanroom facility. The E-beam metal deposition is performed with Mo pellets placed on a crucible. The deposition is performed at a vacuum pressure of 5 e^{-6} Pa. The deposition rate of metal is maintained between 0.1 to 0.5 Å/s. The deposition rate and thickness of the metal deposited are monitored in the rate indicator. A thickness of 100 nm was maintained in all the fabrication processes. The thickness of the sample was validated with profilometric measurements post fabrication. The sheet resistance of the Mo film was measured using Van-der-pauw measurements. The fabricated sensors are stored in Nitrogen desiccator until use. The individual sensors are cut from the substrate for use in biosensing characterization experiments. The form-factor including the non-electrode space area was maintained consistent for all the sensors.

Crosslinker functionalization on Mo electrode

The surface functionalization of crosslinkers is required for efficient immobilization of biomolecules on the sensor surface. The choice of crosslinkers is dependent on the binding affinity with the metal electrode. In this work, two class of crosslinkers have been evaluated for the formation of monolayer of crosslinkers on Mo electrode. The binding affinity of Mo electrode with

thiol and carbodiimide crosslinkers have been characterized through FTIR, XPS and fluorescence microscopy techniques. These experimental results have been described in chapter 5.

Dithiobis (succinimidylproprionate) (DSP) is a thiol based crosslinker which has amine reactive ends (Figure 1). The cleaving of disulphide bond exposes the open sulphur end for binding with metal electrode forming a metal thiol crosslinker monolayer on sensor surface.

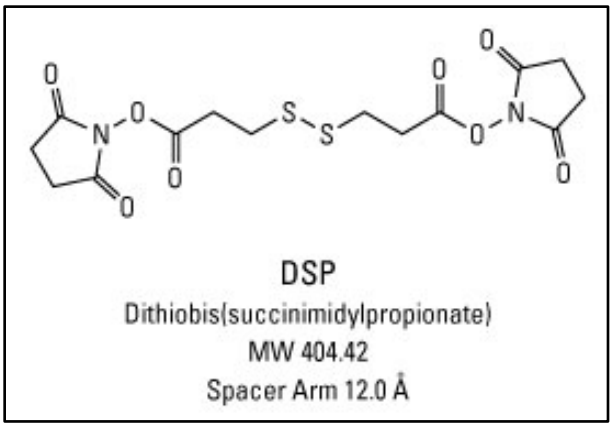

Figure 1. Structure of DSP crosslinker molecule (Reference: Thermofisher scientific)

EDC-NHS crosslinker chemistry consists of two crosslinker molecules 1-ethyl-3-(3-dimethylaminopropyl) carbodiimide hydrochloride (EDC) and N-hydroxysuccinimide (NHS) which are used in combination to form a crosslinker monolayer on electrode surface (Figure 2). The material characterization of the interaction of EDC-NHS crosslinkers with Mo electrode is discussed in Chapter 5.

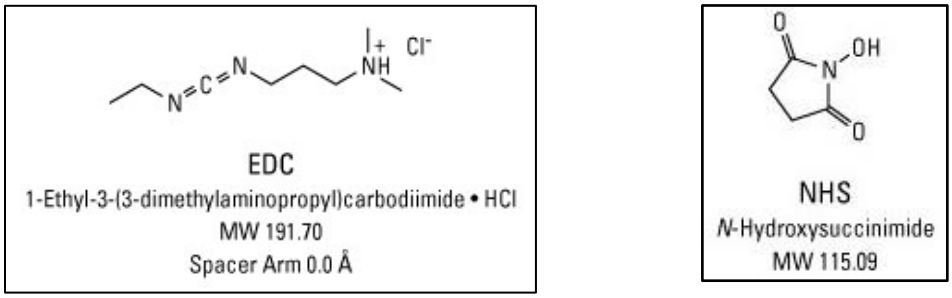

Figure 2. EDC and NHS crosslinker structure (Reference: Thermofisher scientific)

Transduction techniques for biosensing applications

Signal transduction methods help in interpretation of sensor's response from biomolecular binding. Various transduction techniques which have been used for biosensing applications include electrochemical, optical, acoustic and optical-electronic, piezoelectric etc.[25] Among the various transduction methods, electrochemical transducers poses advantages of miniaturization, rapid detection capability and scope for integration with portable hardware devices. Electrochemical transducers are generally potentiometric, amperometric or conductometric. The signal transduction resulting from accumulation of charge at the electrode surface is the basis for development of potentiometric biosensors. The pH electrode is an example of potentiometric biosensors. The absence of bio affinity recognition elements to modulate charge as a result of biomolecular binding event is the primary limitation associated with this technique.

The amperometric transducers are based on measurement of current resulting from electrochemical redox reactions. The magnitude of the current is correlated to the concentration of the electroactive product. The conductimetric transducers are based on the measuring the changes in the conductance at the sensor surface. Impedimetric biosensors are a type of electrochemical transducers wherein the changes in impedance at the surface modified electrode is correlated to the concentration of target analyte. The binding of target biomolecules to the surface functionalized recognition biomolecules at the electrode- electrolyte interface which is transduced as changes in impedance in a faradaic or non-faradaic method depending on the use of redox molecule.

Electrochemical Impedance Spectroscopy (EIS) technique

EIS technique involves the application of an alternating current (AC) voltage to the electrode and measuring the output current from the sensor. The ratio of voltage to current is the impedance of the sensor. An electrical circuit model is modelled to study the biosensor system. For this work, Randles equivalent electrical circuit model (Figure 3) is used for understanding the changes in the electrical parameters occurring at the electrode.[26] The biomolecular binding of proteins causes transient charging at the electrode-electrolyte interface forming an electrical double layer of charges. The transient building of charge causes change in double layer capacitance (C_{dl}). The solution resistance of the buffer is modelled as R_{sol}. The resistance and capacitance contributed by Mo is modelled as a parallel RC circuit group.

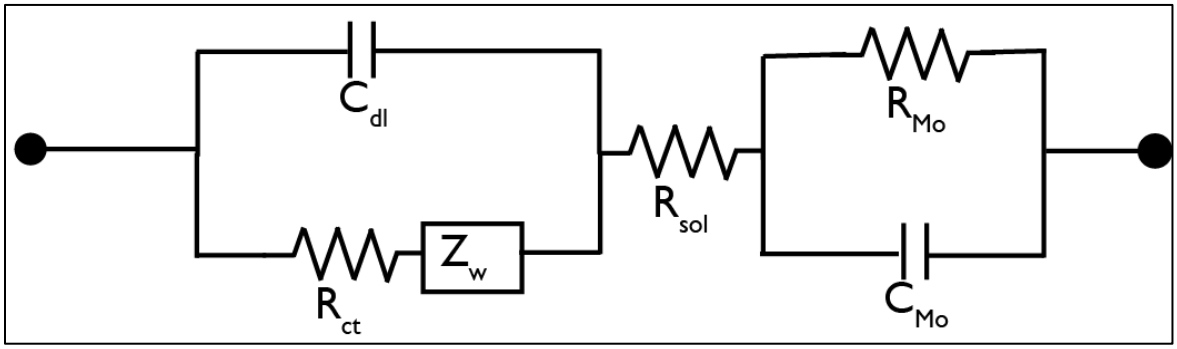

Figure 3. Randles equivalent electrical circuit

The impedance is composed of real and imaginary component depending on the electrical parameters contributing to the change in impedance. The output impedance is correlated to the concentration of target analyte bound to the surface functionalized antibody.

Inflammatory biomarkers detection in urine

Rapid detection of diseases is of critical significance for reducing the deaths occurring from fatal diseases. Non-invasive diagnostic methods are preferred over invasive methods because there is no need for trained personnel to perform sample collection. Non-invasive detection methods consist of physiological monitoring of target biomarkers in physiological fluids such as saliva, sweat, urine, tears etc. The ability to detect disease biomarkers from readily available biological fluids has enabled the development of POC biosensors and wearable sensors thereby enabling real-time monitoring of target biomarkers. With the advances in biosensors, the sample volume requirement has critically reduced thereby further facilitating disease detection from sweat, saliva, tears etc. Urine is one of the important biological fluids which provides valuable information about the physiological state of the body. A number of critical biomarkers are expressed in urine and hence facilitates reliable detection of their elevated expression. Urine contains biomarkers for detection of various diseases related to kidney ailments, cardiovascular diseases, cancer, infectious diseases etc.[27] Urine is also considered as a diagnostic buffer for monitoring the levels of glucose. Thus, the amount of glucose in the urine provides diagnostic and prognostic information about diabetes. Urine consists of critical biomarkers which are relevant to cancer detection. For example, urinary F2-isoprostanes is a biomarker for prostate carcinogenesis. Inflammatory biomarkers such as CRP, IL-6 are prominent biomarkers which are of significance in understanding inflammatory condition in human body. CRP and IL-6 have been assessed as critical biomarkers for many infectious diseases such as periprosthetic joint infection[28], community acquired pneumonia[29] cardiovascular diseases[30], crohn's disease.[31]

Therefore, the early detection of elevated levels of CRP and IL-6 helps in the early detection of many infectious and cardiovascular diseases. Thus, the urine based diagnosis methods provide scope for non-invasive and reliable detection of concentration of inflammatory biomarkers. The restrictions of low sample volumes availability are not relevant for urine based detection methods. IL-6 facilitates the acute phase response in the liver thereby causing the production of CRP.[32] Thus, the detection of both IL-6 and CRP holds significance in rapid detection of various inflammatory and infectious conditions.

CHAPTER 3

NOVELTY OF THE DISSERTATION

Novelty in Electrode Material

This work is focused on evaluating a novel metal electrode namely molybdenum (Mo) for use in affinity based electrochemical biosensors. The demonstration of various oxidation states by Mo facilitates the formation of chemical compounds with varied stoichiometry which is useful for formation of stable chemical conjugates with crosslinkers.

Novelty in Mo-crosslinker interaction

The interaction between Mo electrode and crosslinker molecules was characterized through multiple material characterization methods. The carbodiimide crosslinker binding chemistry was based on leveraging the passive oxide layer on Mo electrode.

Novelty in application to electrochemical dipstick urine biosensor design

The novel crosslinking methods were applied to detect two inflammatory biomarkers in human urine samples namely IL-6 and CRP. The sensor form-factor was designed as a dipstick format on a flexible nanoporous substrate. This work is also a novel demonstration of an electrochemical dipstick biosensor for the detection of inflammatory biomarker from human urine samples. The biosensor is envisioned to be developed as a low-cost home based point of care dipstick biosensor for disease detection in human urine samples.

CHAPTER 4

FLEXIBLE MOLYBDENUM ELECTRODES TOWARDS DESIGNING AFFINITY BASED PROTEIN BIOSENSORS

Prior Publication

This manuscript was published in the MDPI Biosensors Journal in 2016: Kamakoti, V., Panneer Selvam, A., Radha Shanmugam, N., Muthukumar, S., & Prasad, S. (2016). Flexible Molybdenum Electrodes towards Designing Affinity Based Protein Biosensors. Biosensors, 6(3), 36.

The primary goal of this work was to evaluate the feasibility of Mo to be used in affinity based biosensors. The link to the article is http://www.mdpi.com/2079-6374/6/3/36

Abstract

Molybdenum electrode based flexible biosensor on porous polyamide substrates has been fabricated and tested for its functionality as a protein affinity based biosensor. The biosensor performance was evaluated using a key cardiac biomarker; cardiac Troponin-I (cTnI). Molybdenum is a transition metal and demonstrates electrochemical behavior upon interaction with an electrolyte. We have leveraged this property of molybdenum for designing an affinity based biosensor using electrochemical impedance spectroscopy. We have evaluated the feasibility of detection of cTnI in phosphate buffered saline (PBS) and human serum (HS) by measuring impedance changes over a frequency window from 100 mHz to 1 MHz. Increasing changes to the measured impedance was correlated to the increased dose of cTnI molecules binding to the cTnI antibody functionalized molybdenum surface. We achieved cTnI detection limit of 1 pg/ml in PBS

and 1 ng/ml in HS medium. The use of flexible substrates for designing the biosensor demonstrates promise for integration with large-scale batch manufacturing process.

Keywords: molybdenum, bioassay, flexible substrate, cardiac troponin-I, label-free biosensing

Introduction

Point of care diagnostic devices offer efficient and cost-effective solutions for early detection of diseases and monitoring of patient health conditions.[33] Flexible polymers are preferred choice of substrates in the point of care diagnostic biosensing devices owing to their enhanced physiochemical properties. These flexible substrate based biosensors holds promise for mass production thereby aiding in providing disease diagnostic capabilities to resource limited environment.[34] The signal response obtained as a result of affinity based binding between the surface immobilized recognition element and its target conjugate.[35] Affinity based biosensors consist of a biological recognition element such as an antibody or any other type of receptor immobilized on a sensor and integrated with a transducer to detect and measure the concentration of a target bio-analyte. Antibodies are most widely used biological recognition elements in the affinity-based biosensors due to their high affinity to proteins also known as analytes and commercial availability. The binding of the antibody to the antigen at the sensor surface generates a signal response. The phenomenon to detect target analytes through the use of only one capture antibody alone and hence leading to a distinguishable signal is called single-capture immunoassay.[36]

The substrate of the sensor is a crucial component of the biosensor. Silicon has been used for the development of biosensors as it enables precise design of electrodes in the micrometric dimensions using microelectronic photolithographic processes and it favors the integration of signal processing

hardware components on the same substrate.[37] The lack of flexibility of the silicon substrate is the key limiting factor in use in emerging applications such as flexible substrate biosensors. Flexible substrate biosensors can be scaled up to large-scale batch manufacturing processes and possess the advantages of low-cost and easy disposal.[38] A number of polymeric materials have been evaluated for the design of flexible biosensor platforms.[39] Porous nanomembranes are the preferred choice of substrate material in various biosensing applications.[23b, 40] One of the favorable porous substrate polymers is polyamide. Polyamide membranes have been demonstrated as a favorable substrate material for developing flexible substrate biosensors.[41] The presence of pores in the substrate of the membrane based biosensors has been shown to enhance the signal response from the sensor due to the phenomenon of nano-confinement of biomolecules.[24, 42] The nanoporous membranes facilitate the elimination of charge screening caused by the non-specific components in the diffuse region of the electrical double layer. The pores in the membrane are the sites where the biomolecular interactions occur thereby resulting in an enhanced output signal. Polyamide membranes exhibit high mechanical strength and are hydrophilic which favor their use with aqueous solutions. Enhanced signal response is obtained from the nanoporous electrodes with a pore size of the order of 200 nm when compared to planar electrodes for biosensing applications.[43] Gold (Au) has been a preferred choice of electrode material in biosensing applications.[20, 44] However, there is a growing interest in evaluating dichalcogenides for biosensing applications due to their high electron mobility, enhanced surface area to volume ratio.[14a, 45] Molybdenum is transition metal with an electronegativity of 2.16 on the Pauling scale. It does not visibly react with oxygen or water at room temperature[46]. Many of the first-row transition elements have a known biological function and in many cases, redox reactions are linked to their role.[47]

Molybdenum has been used as an bottom electrode material in bulk acoustic resonator applications due to its good electrical conductivity property.[6] The molybdenum electrodes have been demonstrated to form a thicker electrical double layer compared to Nickel and Platinum in the hydrogen production through water electrolysis in 1-butyl-3-methylimidazolium tetra fluoroborate (BMI.BF4) through Electrochemical Impedance Spectroscopy (EIS) technique.[8] Electrochemical interfacial capacitance is defined as the capacitance per surface area and is a function of electrical double layer capacitance.[48] Mo has been demonstrated to exhibit electrochemical behavior upon the interaction with an electrolyte.[49] The presence of interfacial capacitance of Mo can be leveraged for biosensing by enhancing the signal response from binding of biomolecules which is utilized in the EIS technique.[8] The binding between the biomolecule and the electrode surface is of crucial significance for the successful operation of the biosensor. Mo demonstrates a favorable chemistry in binding with sulphur.[50]

The biomolecule chosen for this study is a well-established cardiac biomarker, Troponin-I (cTnI), whose detection in the bloodstream signifies acute myocardial damage. Elevated levels of Troponin-I in the range of ng/ml or higher has been clinically correlated to the onset of myocardial infarction and other cardiac ailments. The enzyme-linked immunosorbent assay (ELISA) and radioimmunoassay (RIA) are conventional methods for monitoring the cTnI levels in a clinical environment.[51] The limit of detection associated with these conventional detection techniques are in the range of ng/ml to μg/ml. In order to detect an early spike in the levels of the cTnI, there is a need for biosensors for detecting lower concentration of the cTnI in a reliable manner. Various biosensing techniques such as electrochemiluminescence[52], faradic electrochemical methods[53],

colorimetric methods[54] have been leveraged to detect the levels of the cTnI. The following table compares the performance matrices of various biosensing techniques:

Table 1. Comparison of immunoassay performance for cTnI detection

Technique	**LoD**	**Dynamic Range**	**Reference**
Electrochemiluminescence	0.0025 ng/mL	0.0025-10 ng/ml	[52]
Faradaic EIS	4.2 pg/mL	0.01-10 ng/ml	[53]
Optomagnetic biosensor	0.03 ng/mL	0.03-6.5 ng/ml	[55]
Colorimetric	0.01 ng/mL	0.01-5 ng/ml	[56]
Surface plasmon resonance	68 ng/L	68 ng/L-660 μg/L	[57]

Electrical biosensing is shown to be more robust than other label free transduction mechanisms due to its speed, sensitivity, ease-of use, and low cost.[58] Electrical biosensing using EIS technique is a powerful technique to monitor the events occurring on the electrode–electrolyte interfaces.[2] EIS technique has been evaluated and applied for the detection of number of bioanalytes.[59] In brief, EIS measurements can be performed in two ways: faradaic EIS and non-faradaic method. Faradaic impedance measurements are usually carried out by using a reversible redox probe while non-faradaic impedance measurements are done without using any redox probe.[60] In a non-faradaic sensor, the capacitance of the electrode–electrolyte interface can be considered as the main indicator of interaction between the antibody and antigen.[61] The non-faradaic biosensors have the advantage of low instrumentation cost and have scope for miniaturization. Thus non-faradic biosensor based on EIS promises scope for development of low-cost point of care diagnostic device for monitoring the levels of cTnI in a reliable manner.

Herein, we presented an easy and facile way to design an affinity based protein biosensor, which has vast scope for integration with a point of care diagnostic device. Conversely, to other previously reported works for cTnI detection, in this paper we demonstrate the detection of cTnI by employing the non-Faradaic method to probe the cTnI concentration changes. We have utilized EIS technique to study the changes in the capacitance due to the interactions of molybdenum electrode and the protein biomarkers. We have demonstrated the feasibility in the use of molybdenum as an electrode material in biosensor for the detection of cardiac biomarkers. The electrochemical property exhibited by the molybdenum upon its interaction with the electrolyte has been leveraged in the design of a non-faradic label-free electrochemical biosensor. The enhanced sensitivity obtained with the use of molybdenum as an electrode material is useful for accurate detection of concentration of cTnI. Thus, we have evaluated the molybdenum electrode as an electrode material in capturing the signal response occurring at the sensor surface due to binding of biomolecules. The change in the signal is predominantly due to the changes in the capacitances associated with the binding of charged biomolecules.

Materials and Methods

Sensor fabrication and characterization

Molybdenum (Mo) electrochemical biosensors were fabricated using e-beam evaporation (99.9% purity Mo crucible) on nanoporous polyamide membrane substrates. Polyamide membranes (GE Healthcare Life Sciences, PA, USA) are flexible, lightweight and hydrophilic whose intercalated nanoporous structure allow the capillary wicking of test sample to the sensing region. The sensing region comprises of two concentric circle electrodes which acts as working and counter/reference

electrodes. The design of the working and the counter electrodes is represented in Figure 4 (A). In a typical biosensing application, the biological molecule is immobilized on the working electrode and the signal resulting from the interaction of biological molecules is sensed from the working electrode. Thus impedance of the counter electrode must be smaller. This is achieved by maintaining the area of counter electrode at least ten times higher than that of working electrode. [62] In order to meet the above design requirement, the ratio between the counter and working electrode's area of the biosensor was designed to be 15:1.

The geometrical pattern of the designed electrodes was transferred on to substrate material using shadow masks with CHA Mark 50 e-gun evaporator in UTD cleanroom. The shadow masks were obtained from acrylic cellulose acetate sheets (Apollo® Copier Transparency Film, Lincolnshire, IL, USA). The rate of deposition was maintained at 0.8 Å/s to achieve a uniform metal deposition and thickness of Mo deposition was maintained at 120 nm. The thickness of the deposition was validated through profilometric measurements. The conformal coating of Mo on polyamide were characterized using Scanning Electron Microscope (SEM) and Energy Dispersive X-ray Spectroscopy (EDAX). The morphological characteristics of material characterization is further discussed in the results section.

The measured resistivity of Mo deposition on polyamide with a 4-point probe source meter was $5.9e^{-4}$ ohm cm while the resistivity prior to the Mo deposition was measured to be 6.6 e^{-2} ohm cm. The low resistivity of the molybdenum surface provides good electrical conductivity and thus is advantageous in achieving an enhanced sensor signal response for biosensing. The electrical contact to the potentiostat is established through alligator clips.

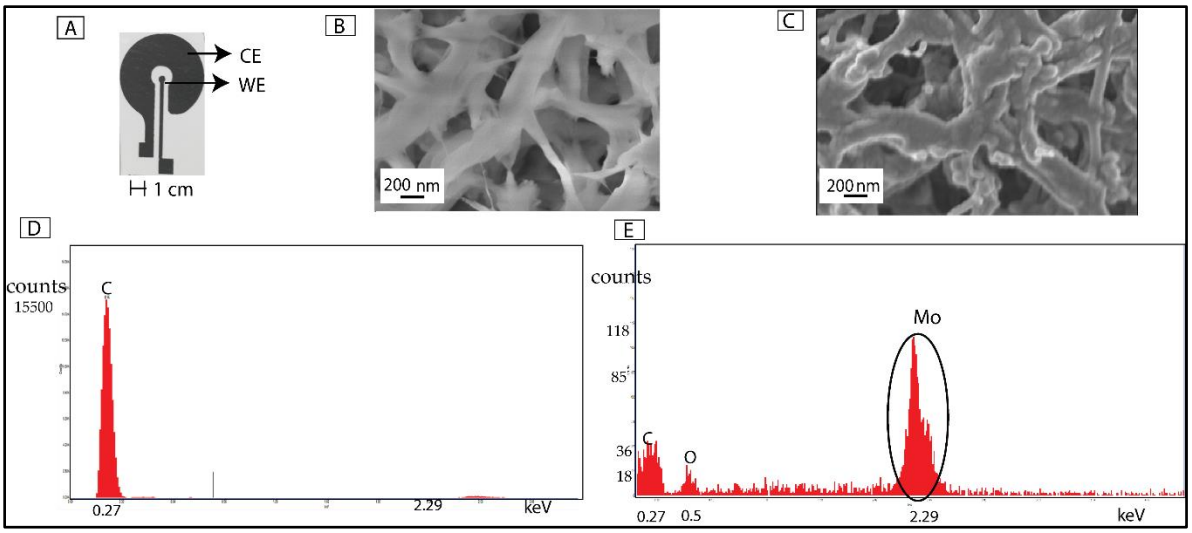

Figure 4. Material characterization of Mo biosensor.

(A) Representation of Mo sensor on polyamide substrate. CE represents the counter electrode and WE represents working electrode; (B) Representation of SEM image of Mo sensor on the porous polyamide substrate before Mo deposition ;(C) Representation of SEM image of Mo sensor on the porous polyamide substrate before Mo deposition; (D) Representation of EDAX spectrum analysis on PA membrane before Mo deposition; (E) Representation of EDAX spectrum analysis on the Mo sensor. The encircled region on the EDAX spectrum indicates the peak corresponding to the L-shell energy peak of the Mo.

Surface functionalization of sensor

Dithiobis succinimidyl propionate (DSP) (Sigma-Aldrich, St. Louis, MO, USA) was dissolved in dimethyl sulfoxide (DMSO) (Sigma-Aldrich, St. Louis, MO, USA) to formulate a 10mM mixture. 30 µL of the DSP-DMSO mixture was added to the Mo electrochemical sensor to allow functionalization of this thiol-based linker molecule on Mo surface and incubated for four hours. 0.15 M 1x PBS buffer was added to the sensor to prepare the surface prior to addition of the

antibody. Monoclonal anti-cTnI antibody stock solution was diluted to 1μg/ml in PBS buffer and then immobilized on the DSP functionalized sensor surface and incubated for 15 minutes. The concentration of antibody to be used was determined through antibody saturation study. The antibody saturation study experiment was conducted with varying antibody concentrations from 100 fg/ml to 1 μg/ml and the change in impedance with respect to a blank PBS sample was studied for the various antibody concentrations. The noise estimation post the antibody conjugation was studied by analyzing the impedance of the sensor for multiple PBS washes following the antibody conjugation. EIS measurements were taken after each assay step with Gamry Reference 3000 potentiostat (Gamry Instruments, Warminster, PA, USA) to validate the binding.

2.3 Calibration dose response analysis for cTnI detection

In order to evaluate the baseline sensor performance on an antibody conjugated sensor, blank buffer devoid of any antigen was added to the sensor. EIS measurements were performed after two minutes of addition of buffer. This measurement was considered as the zero-dose measurement. The impedance at the subsequent antigen concentrations was compared against the zero-dose impedance values. The cTnI antigen was diluted to the experimental concentrations in the target test buffers, PBS or human serum (HS) (Fitzgerald, Acton, USA).After the addition of antigen sample, the sensor was incubated for 15 minutes to allow for sufficient time for binding of antigen with the surface functionalized antibodies. EIS measurements were performed after the incubation time in order to validate the binding of antigen to the surface conjugated antibody. We tested the cTnI antigen concentration from 100 fg/ml to 10 μg/ml in PBS medium and from 100 pg/ml to 10 μg/ml in the HS medium. The dissociation constant between the cTnI antibody and the cTnI antigen is in the range of 10-10 M.[63] In order to validate the binding of the biomolecules on the

porous substrate, we performed the negative control dose response experiment with Bovine serum albumin (BSA) protein.

EIS technique for label-free biosensing

The technique of single capture immunoassay (primary antigen-antibody interaction in the absence of secondary antibody) was leveraged to achieve protein binding and subsequent detection process. The binding of the biomolecules onto the molybdenum electrode perturbs the inherent charge distribution in the electrical double layer (EDL). The perturbation in the charge distribution leads to capacitance changes in the EDL. Thus, the capacitance introduced by the bimolecular binding was measured by the EIS technique. The equivalent electrical circuit is depicted in the Figure 5(B). The EIS technique used in this study is a modification of the standard electrochemical impedance spectroscopy technique wherein redox probes are used to study the interactions occurring at the surface probe. The absence of the use of the redox probe in the implemented sensing system makes it a non-faradic sensor. The electrical stimulus is applied across the electrode in order to direct the surface-charged biomolecules towards the sensing region of the biosensor. The resulting impedance is calculated using the voltage-time function equation as given below:

$$Z = \frac{V(t)}{I(t)} = \frac{V_0 \sin(2\pi f t)}{I_0 \sin(2\pi f t + \phi)}$$

In the above equation, V_0 and I_0 represent the peak voltage and the current signals, 'f' represents the frequency of the applied signal,'t' represents the time and 'ϕ' represents the phase shift between the voltage-time and the current-time functions. When the impedance measurement is carried over a spectrum of frequencies, the technique is referred to as impedance spectroscopy. The binding of the biomolecules causes a change in the output capacitance across the sensing region of the

molybdenum biosensor. The output impedance consists of resistive and capacitive components. The capacitive component indicates the differential surface charge at the EDL as a function of antigen-antibody binding. The parameters of the input voltage namely the amplitude of the sinusoidal voltage and the frequency of the input signal need to be optimized in order to capture the changes in the impedance occurring as a result of binding of biomolecules. The alternating current (AC) input voltage is of the magnitude of 10 mV and the range of test frequency was varied from 100 mHz to 1 MHz. The application of input AC voltage causes the ions in the solution to get attracted towards the molybdenum electrode surface, which is known as inner Helmholtz plane (iHP). The outer Helmholtz plane (oHP) is constituted with ions which facilitate the functionalization of linker molecule onto the sensor surface. The length between the iHP and the oHP is regarded as the length of the EDL. The length of the electrical double layer extends from the iHP as the immunoassay is built on the sensor surface. Figure 5(A) represents the diagrammatic representation of the immunoassay.

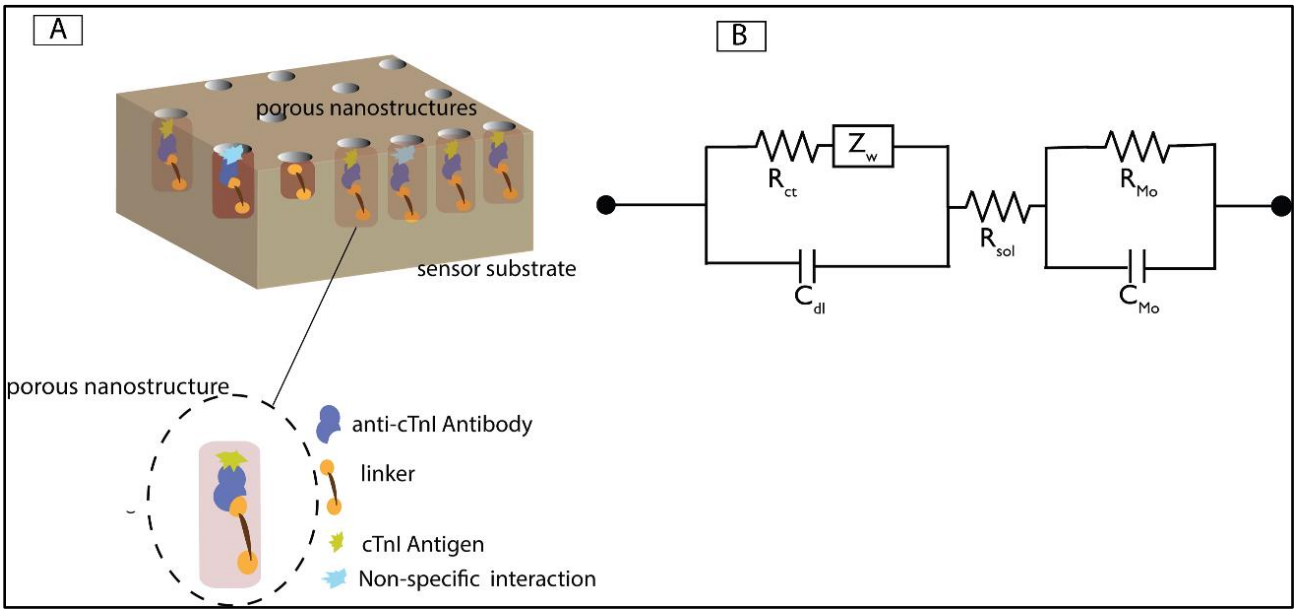

Figure 5. Biosensor design and electrical circuit model

(A) Schematic representation of immunoassay of the Mo biosensor indicating the deposition of Mo on the pores of the membrane. The enlarged segment indicates the building of immunoassay on the pores ;(B) Schematic representation of the equivalent circuit of the Mo biosensor. C_{dl} represents the double layer capacitance dominated by biomolecular binding. R_{sol} represents the resistance contributed by the solution, Z_w represents the Warburg Impedance and Rct represents the charge transfer resistance, R_{Mo} represents the resistance at the Mo electrode, C_{Mo} represents the interfacial capacitance at the Mo electrode surface.

Results

Material characterization of Mo deposition

The material characterization of sensor surface performed with the SEM indicate the deposition of molybdenum on the porous polyamide substrate. Figure 4(B) and Figure 4(C) indicate the SEM images pre and post Mo deposition on polyamide membrane respectively. The SEM micrograph post the Mo deposition validate the conformal deposition of Mo on the pores of the membrane substrate. The profilometry results post the Mo deposition validate the depth of the Mo deposited and its correlation with the preset value.

Figure 4(D) and 4(E) shows the EDAX spectra related to highlighted zone in the SEM micrographs. The objective of measuring the EDAX spectra is to investigate the presence of elements. The distinct peak at the energy level 2.29 keV corresponds to the L-shell energy level of Mo thereby indicating that the deposited film on porous polyamide membrane is molybdenum. The other significant peaks are of Carbon and Oxygen. The hydrocarbon side chains of the polyamide membrane are the probable source. The EDAX spectra on blank polyamide substrate does not indicate any peak correlating to the Mo. The exact nature of deposited film cannot be evaluated using EDAX analysis. However, the presence of molybdenum deposit is certain. Polyamide favored rapid fluid wicking which facilitated the uniform distribution of sample solutions on the electrodes.

Baseline electrical characterization

The baseline sensor response refers to the study of material and electrical properties of the sensor in the absence of biomolecules. This study was performed in order to analyze the effect of inherent

material and electrical properties of the Mo sensor. The baseline electrical properties of the Mo electrode biosensor was studied with EIS technique by the application of an AC voltage of 10 mV at 1000 Hz frequency as the electrode characteristics are studied as part of the bulk properties of the electrode which are studied at the high frequencies.[59] The lower frequencies reflect the effect of biomolecular binding on the electrical double layer. Hence the performance of the immunoassay was evaluated at 1 Hz frequency. The open-circuit impedance in the absence of any fluid on the sensor surface was measured to be 75 MΩ and the short-circuit impedance was measured to be 5224 Ω. A total of n=3 replicates was performed and a coefficient of variation (CV) of 8 % was observed. The low percentage in the CV indicates that the baseline performance of the sensor shows that the sensor stack was reliable for EIS biosensing.

Antibody saturation study

The concentration of the antibody required to completely saturate the sensor surface functionalized linker sites is crucial in order to competitive binding of free linker sites with other biomolecules. We performed the antibody saturation experiment in order to determine the concentration of antibody required for saturating the linker functionalized sensor surface. The experimental conditions for this study was set at 10 mV AC voltage and 1 Hz frequency. A total of n=3 replicates of measurements were performed for this study and the results are represented in Figure 6 (A). The concentration of the antibody at which there is minimal change in impedance compared to earlier concentration is regarded as the saturating antibody concentration. The noise threshold was calculated from the difference in impedance value between the PBS step post DSP functionalization and another blank PBS buffer dose step and was determined to be approximately 3200 Ω. The change in impedance for the lowest antibody concentration of 1 ng/ml was measured

to be 8900 Ω. The change in impedance for antibody concentration of 1000 ng/ml with respect to the baseline PBS measurement was approximately 20 kΩ. The change in impedance with respect to the earlier concentration was negligible and hence 1000 ng/ml was the saturating concentration of the antibody required to complexly saturate all the available linker sites for the antibody conjugation. Thus, the saturating dose concentration for the cTnI antibody was considered to be 1000 ng/ml. Figure 6(B) represents the results of the baseline sensor characterization for multiple PBS wash steps following the antibody conjugation. A total of n=3 replicates were performed and a p value greater than 0.05 was obtained for all the PBS wash steps with respect to the impedance value obtained after antibody conjugation. Thus, the biosensor demonstrates stable measurements post the antibody conjugation after the buffer wash steps. The stable values in the impedance obtained post the PBS wash steps validates the conjugation of antibody to the linker sites and the PBS wash steps does not dissociate the antibody from the sensor surface.

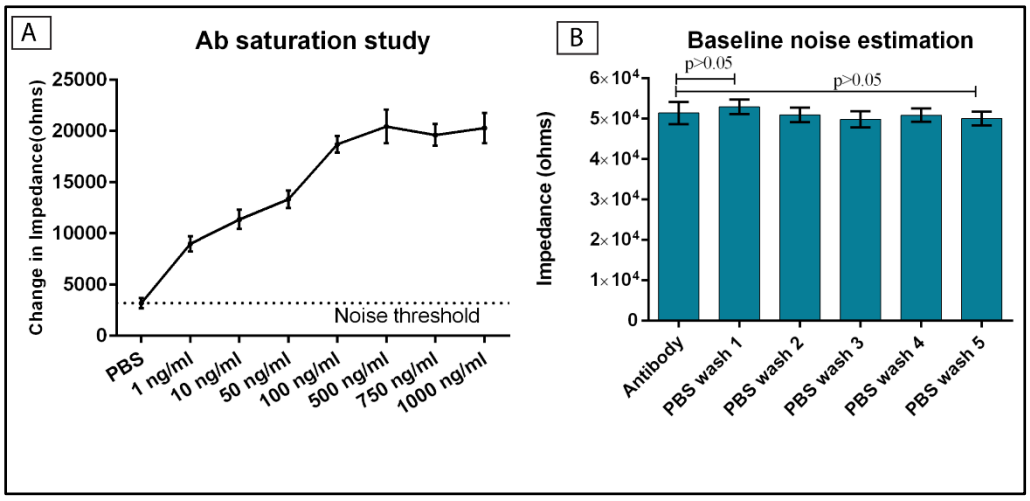

Figure 6. Antibody conjugation analysis

(A) Analysis of antibody saturation study on the DSP functionalized Mo sensor. The dotted line indicates the noise threshold. Error bars indicate the standard error of mean from n=3 replicates;

(B) Baseline noise estimation on antibody conjugated biosensor and multiple PBS wash steps post the Ab conjugation. The impedance values for the PBS wash steps are statistically insignificant compared to the impedance obtained post the antibody incubation.

Calibration dose response study

The calibration dose response study experiments were performed for a frequency range of 100 mHz to 1 MHz frequency with 10 mV (peak to peak) voltage. Figure 7(A) represents the change in the phase angle of the impedance as a function of frequency and Figure 7(B) represents the change in the modulus of impedance as a function of frequency. A lag in the phase between the input voltage and the output current is observed for the different assay steps. The phase lag is contributed by the change in the capacitive elements in the biosensor. The transient building of charges occurs at the electrical double layer as a result of biomolecular binding. The maximum phase for the DSP functionalized sensor was measured to be approximately 20˚. The phase of the sensor increases with the subsequent assay steps due to increase in the capacitance at the molybdenum electrode due to the biomolecular binding. The phase of the system increases up to approximately 58˚for the cTnI antigen concentration of 10,000 ng/ml. The changes in the phase with respect to the assay steps were significant. These significant changes in the phase indicate the presence of capacitive binding. The maximum changes in the phase between the DSP functionalization step and the subsequent assay steps were observed at 1 Hz frequency and hence the calibration dose response analysis were performed for impedance values at 1 Hz frequency. Since the maximum phase changes are observed at a frequency of 1 Hz, it is inferred that the capacitive behavior of the biosensor is dominant at this frequency. At high frequencies, the phase of the signal approaches zero for all the assay steps. Also, at higher frequencies, the impedance

curves associated with the Bode magnitude analysis overlap with each other. Hence, the low frequency region (1 Hz) is chosen to study the distinguishability in the doses as a function of impedance. The impedance of the biosensor decreases with increase in the frequency of the input signal. For instance, the impedance value at 100 mHz for 10 ng/ml is 45 kΩ and it decreases up to 975 Ω at 1000 Hz frequency. The changes in the impedance for various concentrations of the antigen were distinguishable from each other. Thus, these distinct changes in the impedances for various antigen concentrations validate the binding between the surface functionalized antibody with the antigen molecule.

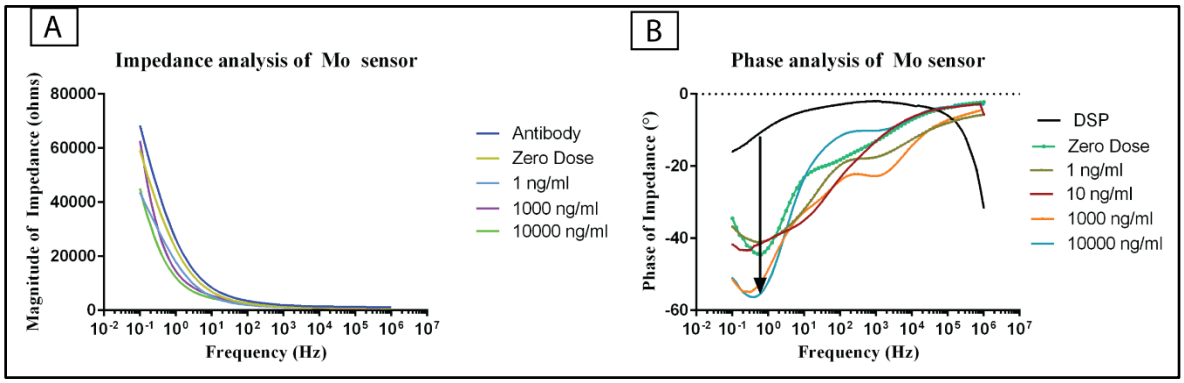

Figure 7. Magnitude and Phase analysis of Mo sensor

(A) Magnitude of impedance of Mo sensor. The magnitude of the impedance decreases with increasing antigen concentrations; (B) Phase analysis of Mo sensor. Maximum phase changes between the DSP functionalization step and subsequent assay steps were observed at 1 Hz frequency.

Figure 8(A) and 8(B) represent the results of calibration dose response experiments for cTnI protein detection in PBS and HS medium respectively at 1 Hz frequency. The percentage change in impedance with respect to the zero dose for the lowest antigen dose of 100 fg/ml was 8%. The impedance difference with respect to the zero-dose measurement was calculated to be 3 kΩ. The

% change in impedance increased with higher concentrations of the antigen. For the cTnI concentration at this concentration of 10,000 ng/mL, the % change in impedance was approximately 60 % and the change in impedance with respect to zero-dose sample was calculated to be 29 kΩ.

The control experiments with the BSA protein did not yield an increasing trend in the change in impedance percentage. The change in impedance with respect to zero-dose for the control doses were measured to be less than 10%. The change in the impedance for the control doses is attributed to the change in the diffusion driven impedance at the Mo electrode electrolyte interface.

The decrease in the impedance after the antigen binding is in correlation to the increase in the double layer capacitance due to the binding event. Thus, the percentage change in impedance increases with higher cTnI concentration. The increase in the change in the impedance for higher concentrations observed for the cTnI antigen concentrations indicate the signal from the sensor is a result of specificity in binding between the cTnI antigen and the cTnI antibody. The signal to noise ratio for an immunoassay assay is fixed at 3.[64] Based on the analysis of the results of the calibration dose response, the difference in impedance between the impedance for dose concentration and that of negative control was measured to be 600 ohms and this value is referred to as noise threshold for the calibration dose response study. The specific signal threshold (SST) is calculated as three times the noise impedance and was measured as 1800 ohms. In the Figure 8 (A), the percentage change in impedance for the cTnI concentration of 100 fg/ml was less than the noise threshold. The lowest concentration of cTnI antigen which was above the impedance at the noise threshold is regarded as the limit of detection (LoD) for the sensor. In our work, the LoD of

the sensor is inferred to be at 1 pg/ml in PBS medium. The dynamic range of detection in the PBS medium was from 1 pg/ml to 10 µg/ml.

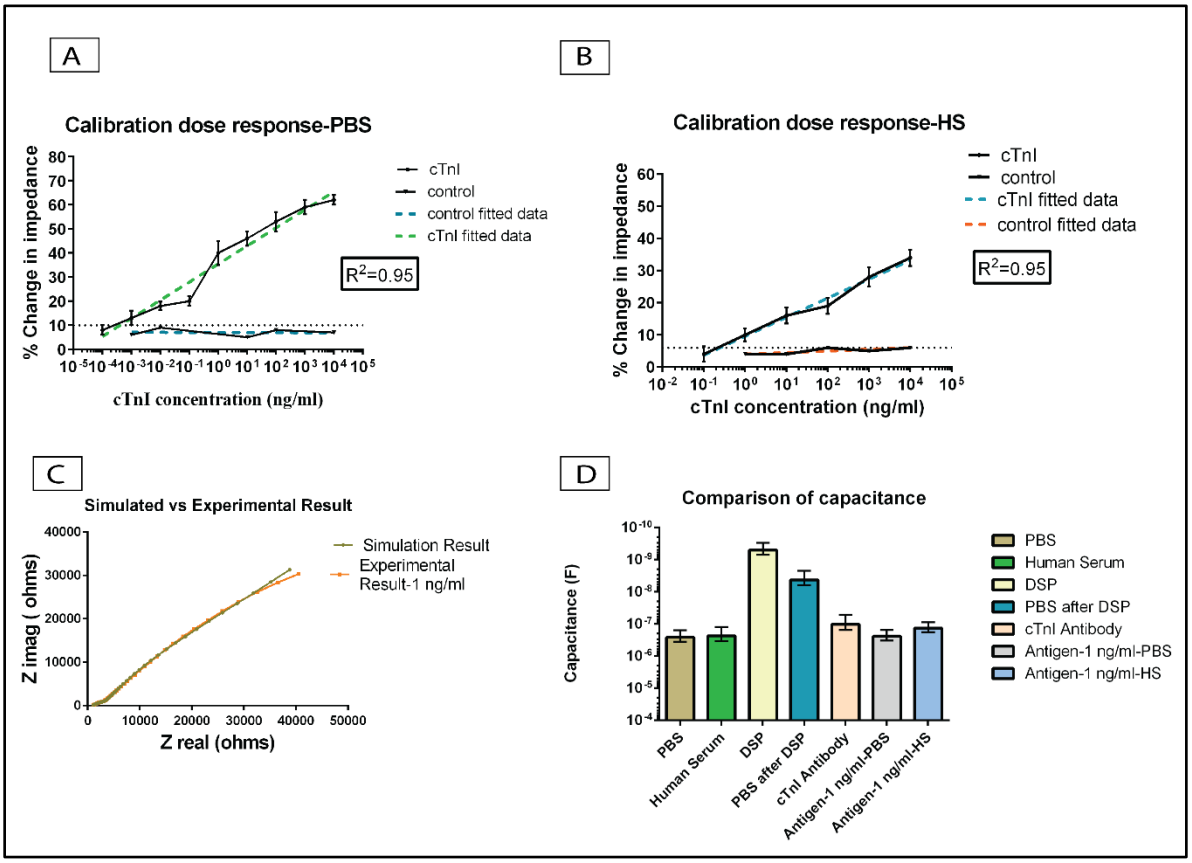

Figure 8. Calibration dose response analysis on Mo sensor

(A) Calibration dose response analysis in PBS medium. The dotted line indicates the noise threshold. The LoD for the sensor in the PBS medium is 1 pg/ml. (B) Calibration dose response analysis in HS medium. The LoD for the sensor in HS medium is 1 ng/ml. Error bars represent the standard error of mean from n=3 replicates.(C) Comparison of experimental vs simulated result for 1 ng/ml of cTnI antigen.(D) Comparison of capacitance for various assay steps on Mo biosensor.

In order to simulate a diagnostic sensor environment, we tested the immunoassay in HS medium for cTnI detection. The experimental concentrations of the cTnI antigen was diluted in the human serum medium and was tested on the antibody conjugated molybdenum electrode biosensor. The percentage change in impedance for the cTnI concentration of 100 pg/ml with respect to a zero-dose measurement with blank human-serum alone was measured to be 4%. This value lies within the noise threshold region. The lowest cTnI concentration which is above the noise threshold is 1 ng/ml. Hence the LoD for the sensor in the HS medium is 1 ng/ml. The change in impedance increased with increase in the antigen concentration. The percentage change in impedance for 10,000 ng/ml cTnI concentration with respect to zero-dose measurement was measured to be 34%. The increase in the percentage change in impedance for increasing concentration of the antigen is an indication of increase in the double layer capacitance due to the binding of the biomolecules at the Mo electrode surface despite the presence of interfering biomolecules present in the human serum. The dynamic range of detection in the human serum medium was from 1 ng/ml to 10 μg/ml. The change in impedance for the control experiments with BSA protein were less than 7 % with respect to zero-dose measurements. The negligible change in percentage for the negative doses indicates the specificity in the binding between the cTnI antigen and the cTnI antibody. Figure 9 (C) represents the comparison of Nyquist plot between the experimental result obtained for the 1 ng/ml cTnI antigen concentration and the simulated value. The simulated values were obtained after fitting the experimental data into the equivalent circuit as shown in Figure 9(B). The simulated data points correlated to the experimental values with a low chi square value of 4.96 e-^{6}. Thus, the presence of interfacial capacitance is validated in the derivation of equivalent electrical circuit for the biosensor. The value of interfacial capacitance for the Mo obtained from simulation

analysis was obtained to be 5 μF. Figure 9(D) represents the comparison of experimentally measured capacitance values for various immunoassay conditions at Mo electrode. The measured capacitance increased from the DSP step to the antigen binding step thereby validating the capacitive binding between the biomolecules.

Optical readout for cTnI detection

In order to demonstrate the reporting the sensing of cTnI molecules in a user-friendly format, we developed a LED based prototype to indicate the of cTnI antigen. Figure 9 (A) indicates the cTnI antibody immobilized sensor. The LED prototype operates similar to a Boolean logic output indicating a change in the output for the impedance value correlating to the 1 pg/ml cTnI concentration. The simple LED prototype supports the favorability of molybdenum biosensor to be integrated with electrical circuit components. The threshold concentration to trigger the output response is preset as a correlation to an impedance value. The output LED glow is an indication of crossover point of the cTnI concentration. Figure 9(B) indicates ON state of the LED after the addition of cTnI antigen. The addition of the antigen on the antibody-immobilized sensor decreases the impedance of the circuit. A comparator integrated circuit compares the impedance with a preset threshold value and completes the circuit to glow the LED. We observed that the output LED turned ON within 10 seconds of addition of the antigen of 1 pg/ml concentration. The rapid change in the output from the sensor indicates that Mo facilitates the charge conduction through the porous substrate. The reader can be extended to classify the cTnI concentration into multiple classification segments.

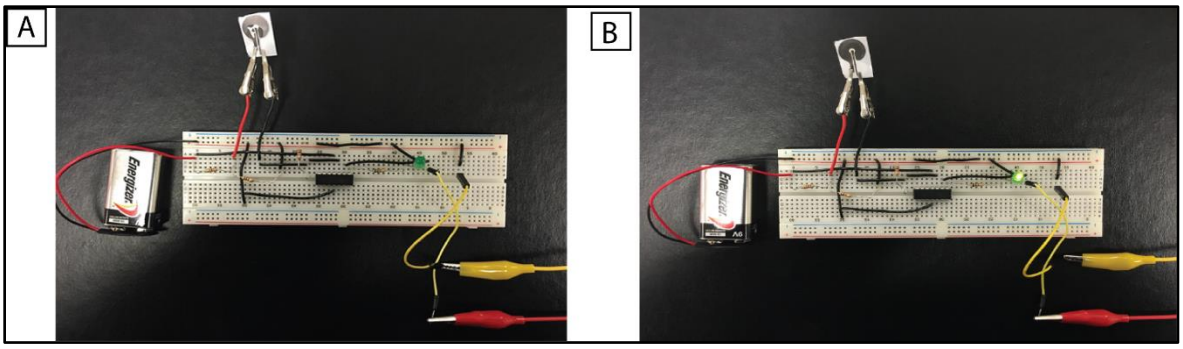

Figure 9. Electrical prototype of an optical reader for cTnI detection

(A) Optical reader indicating an "OFF" output state on an antibody conjugated sensor.(B) Optical reader indicating an "ON" state upon the addition of antigen sample. The binding between of biomolecules decreases the impedance below the threshold value thereby turning the output LED to "ON" state.

Discussion

We have leveraged the material properties of the molybdenum for use as an electrode material for the design of a cardiac biomarker (cTnI) detection biosensor. The flexibility of the polyamide substrate offers scope for integration of the biosensor with textile based point of care diagnostic platform. The presence of peaks in the EDAX spectrum analysis correlated with the energy levels of the Mo validates the conformal deposition on the polyamide substrate. SEM images of the Mo sensor represents the deposition of Mo on the porous polyamide membrane. The decrease in the impedance after the DSP incubation indicates that the Mo electrode surface exhibits affinity towards thiol linker molecule. The self-assembled monolayer formed at the sensor surface forms the stack upon which the biomolecules are immobilized. The linear increase in the change in the impedance of up to 20 kΩ for saturating antibody concentration of 1 µg/ml elucidates the binding

between the antibody and the linker functionalized Mo electrode sensor surface. The increase in the change in the impedance is the results of the change in the double layer capacitance element at the interface of the Mo and the electrolyte. The phase of the biosensor increases up to 58° for the antigen concentrations. The increase in phase lag is due to capacitive binding at the pores of the polyamide surface.

The biosensor exhibited clear distinguishability in the impedances for various concentrations of the cTnI antigen at 1 Hz frequency. The change in the impedance is theoretically to the double layer capacitance element of the equivalent electrical double layer model (C_{dl}). Molybdenum electrode facilitates the changes in the capacitance associated with the binding event between the surface conjugated antibody and the target antigen present in the sample. The changes in the impedance is predominantly driven by the changes in the capacitance occurring due to biomolecular binding. Mo electrode deposited on the porous polyamide substrate facilitates the capacitive binding between the biomolecules.

The biosensor showed a linear response over a broad detection range from pg/ml to µg/ml with approximately 60 % change from the zero-dose impedance measurement in the PBS medium and a change of 35 % in HS medium. The increase in the percentage change in impedance for higher sample concentrations validate the biomolecular binding. The lower limit of cTnI detection in the PBS medium is 1 pg/ml as its change in impedance was higher than the noise threshold set by the control (BSA) protein concentrations. The lower limit of detection in the HS medium was 1 ng/ml. The small change in impedance for the negative control samples is attributed to the diffusion driven Warburg impedance (Z_w). The increase in the measured capacitance with the immunoassay steps indicates that the molybdenum electrode drives the change in the double layer capacitance at the

electrical double layer formed at the sensor surface thereby favoring the detection of precise changes in the cardiac troponin levels. The use of flexible substrate is advantageous for its scope for large-scale scalability in the biosensor fabrication. The sensors are disposable after one time use and hence holds promise for integration with a point of care diagnostics device.

Conclusions

The electrochemical behavior of the Mo has been leveraged in building a label-free biosensor on a flexible membrane substrate. The biosensor demonstrates feasibility of cTnI detection in PBS and HS medium over clinically relevant concentrations for the cTnI detection. The efficient biomolecule detection capability of the molybdenum biosensor in the human serum despite the presence of interfering biomolecules supports the claim of molybdenum as an economically attractive alternative to the gold as an electrode material in diagnostic biosensors. Thus, the molybdenum electrode biosensor has immense scope for use a portable point of care diagnostic biosensor with ability to detect the onset of cardiac disease in a reliable and rapid manner.

CHAPTER 5

INVESTIGATION OF MOLYBDENUM-CROSSLINKER INTERFACES FOR AFFINITY BASED ELECTROCHEMICAL BIOSENSING APPLICATIONS

Prior Publication:

This manuscript has been submitted to the Applied Surface Science journal and is currently under review. The primary objective of this work was to evaluate the interaction of crosslinkers with molybdenum electrode.

Abstract

The electrochemical properties of molybdenum (Mo) has been investigated for implementation as an electrode material for affinity based biosensing towards developing flexible electronic biosensors. Treatment of the native oxide of molybdenum was investigated through two surface treatment strategies namely thiol and carbodiimide crosslinking methods. The binding interaction between cross-linker molecules and Mo electrode surface has been characterized using Fourier Transform Infrared Spectroscopy (FTIR), X-ray photoelectron spectroscopy (XPS) and optical microscopy. The efficacy of treatment of Mo with its native oxide using carbodiimide cross linking methodology was established. The carbodiimide cross-linking chemistry was found to possess better surface coverage and binding affinity with molybdenum electrode surface when compared to thiol cross-linking chemistry. Electrochemical characterization of Mo electrode using Electrochemical Impedance Spectroscopy (EIS) and Cyclic Voltammetry (CV) techniques was performed to evaluate the effect of ionic properties of solution buffer on the Mo electrode's

performance. Affinity based biosensing of C - reactive protein (CRP) has been demonstrated on a flexible nanoporous polymeric substrate with detection threshold of 100 pg/ml in synthetic urine buffer medium. The biosensor has been evaluated to be developed as a dipstick based point of care device for detection of biomarkers in urine.

Introduction

Experimental techniques that interface biomolecules directly with microelectronic systems are increasingly being used in a wide range of diagnostics applications. The search for better diagnostics technologies has been directed down to two interrelated pathways. One is the continuing efforts to develop the lab on a chip concept, particularly for detection of biomolecules, and this reflects the general trend in biotechnology where standard assays are being replaced by molecular testing.[65] The second is the development of porous polymer-based analytical devices which have the advantage that polymeric materials can be machined in similar ways to silicon but it is much cheaper, and an important consideration for devices in the developing world.[66] In the realm of porous polymer based analytical devices there has been significant emphasis on the fluidics aspect but not sufficient emphasis has been placed in the material systems utilized for achieving sensing/testing.[67] Mo has frequently been selected as the electrode material to minimize the acoustic attenuation and provide good electrical conductivity, it has been primarily applied for acoustic resonator applications.[68] In this paper, we have evaluated the suitability of molybdenum as an electrode material for polymeric substrates. We have investigated surface functionalization strategies for molybdenum towards designing electrochemical biosensors suitable for implementation in polymer based porous bioanalytical devices. These devices lend themselves to be integrated into dipstick formats enabling rapid biosensing.

Dipsticks for urinalysis are a convenient diagnostic tool as they are non-invasive, extremely portable, and very cheap to manufacture.[69] Unfortunately, the accuracy of the results is highly dependent on multiple stringent requirements which include sample preparation, correct interpretation of a gradient colour scale, and readout timing.[70] There is an opportunity to remove these stringent requirements through electronic dipsticks may be designed to report the concentration of a specific biomarker from urine in a manner similar to blood glucometer. One challenge in converting colorimetric dipsticks into electronic dipsticks is the choice of the electrode material and the electrochemical assay that is incorporated onto the electrode. Standard electrochemical assays typically utilize gold/ platinum as electrodes. These choices typically increase the cost of a dip stick thus pricing the assay outside of considerations for implementation in developing economies. In order to achieve this overarching goal, in this publication we have investigated a novel material system namely molybdenum (Mo) as an electrode for designing electronic dip sticks for evaluating biomarkers from urine.

The electrochemical properties of molybdenum (Mo) and its compounds have been demonstrated in their use as in electrocatalytic applications.[71] Mo exhibits various oxidation state ranging from II to +VI. The wide range of oxidation states facilitates the formation of stable chemical interactions with various organic and inorganic functional groups.[5] Mo and its compounds have widely been used in battery applications owing to their electrochemical properties.[72] Mo demonstrates electrochemical properties upon its interaction with electrolytes.[73] It is susceptible to formation of passive surface oxide layer.[74] The native oxide layer on Mo acts as a passivation layer thereby facilitating anti-corrosion properties.[75] The biocompatibility and favourable mechanical properties of Mo justify its application as an alloying material in medical implants.[76]

These properties favour the evaluation of Mo as a stable electrode material but fraught with the challenge of utilizing the passive oxide layer towards developing functional biosensors. The passive oxide requires surface engineering to develop a functional molybdenum surface suitable for conjugation of biomolecules.

Engineering the electrode surface for biomolecule conjugation is a critical step towards evaluation of the electrode material for affinity based biosensing applications. Various electrode surface modification strategies such as physisorption[77], enzyme entrapment[78] and covalent attachment[79] have been evaluated for functionalization of biomolecules. Stability of binding of biomolecules to the surface of the electrode enables the successful signal transduction from biomolecular binding to the electrodes. High binding strength resulting from covalent attachment of cross-linkers with electrode surface favours their application in development of affinity based biosensors. The chemical interactions of thiol group based cross-linkers is widely studied in surface functionalization methods.[80] The high binding affinity of Au-S bonds was used for building a stable monolayer suitable for functionalization of biomolecules.[81] Carbodiimide chemistry is another class of cross-linkers, which are also widely reported in the development of biosensors. [82] Surface treatment of molybdenum plays an important role in utilizing its electrochemical properties towards designing polymer based analytical devices.

In this work, we have investigated two methods of surface treatment widely used in affinity based biosensing systems and adapted them towards implementation on molybdenum surfaces with passive native oxide. Due to the integration of molybdenum electrodes onto polymer-based substrates, standard etching based surface treatments are unsuitable for implementation.[83] Hence, we investigated the novel approach of leveraging the native oxide towards designing surface

suitable for biomolecule immobilization. We investigated the utilization of thiol and carbodiimide linker molecules towards surface treatment of molybdenum native oxides and have studied the interaction between Mo and the cross-linking molecules through ATR- FTIR, XPS and optical methods. We have demonstrated the development of reliable multi-layers of cross-linkers for efficient functionalization of capture biomolecule receptors (antibodies). Affinity based bio sensing phenomena on polymer membranous substrates is demonstrated using C-reactive protein (CRP) as a biomarker. CRP is widely studied and reliable biomarker for inflammatory and cardiac diseases[54]. It is expressed in serum and urine.[84] The occurrence of inflammatory disease conditions causes elevated expression of CRP as high as 0.86 mg/L in urine.[85] The effect of ionic properties of buffer on Mo electrode was evaluated through cyclic voltammetry technique. The detection of CRP has been evaluated in synthetic urine buffer through electrochemical impedance spectroscopy.

Experimental Section

Materials and reagents

Glass substrates, (dithiobis (succinimidyl propionate)) (DSP), dimethyl sulfoxide (DMSO), and ethanol were purchased from Thermo Fisher Scientific (MA, USA). N-hydroxysuccinimide (NHS), 1-ethyl-3-(3-dimethylaminopropyl) carbodiimide hydrochloride (EDC), 2-(N-Morpholino) ethanesulfonic acid (MES, pH 3), phosphate buffered saline (PBS, 0.1 M, pH 7), Human serum (HS), Rhodamine 123, potassium hexacyanoferrate (III) ($K_3Fe(CN)_6$) were obtained from Sigma Aldrich (MO, USA). α-CRP antibody and CRP antigen were procured from Abcam (MA, USA). Synthetic urine (pH 6.3) was prepared freshly using the recipe published in previous

studies. Acrylic cellulose acetate sheets were obtained from Staples (TX, USA). All solvents and reagents were of analytical grade and used as received.

Fabrication of Mo biosensor

A three electrode electrochemical configuration was used for evaluation in this work. The schematic of a fabricated Mo biosensor is shown in Figure 10. Desired electrode pattern designed using AutoCAD was translated on to the sensor substrate using shadow masks. Acrylic cellulose acetate sheets with 0.5 inches thickness served as shadow masks and deposition of electrode materials were performed using e-beam evaporation. Ratio of WE to CE surface area was maintained at 3 in order to observe maximum signal response from the working electrode.[62] The working electrode (WE) and counter electrode (CE) consisted of 25 nm Cr/125 nm Mo and reference electrode consisted of 25 nm Ti/125 nm Pt. Post deposition, the fabricated Mo biosensors were stored in a nitrogen desiccator until further use.

Functionalization of Mo biosensor with crosslinker molecules

The binding interactions between Mo and organic molecule were evaluated using two crosslinkers namely DSP, an organic molecule with thiol functional group and well-known EDC-NHS, a molecule with carboxylic acid functional group. In a typical functionalization procedure, fabricated Mo samples were washed with methanol and dried under nitrogen before treatment with crosslinker molecules. Functionalization with thiol molecules involved treatment with 10 mM DSP dissolved in DMSO at room temperature for an hour followed by 3x wash with DMSO to remove any unbound DSP molecules. Similarly, functionalization with carboxylic acid group was achieved by treating Mo samples with 400 mM of EDC and 100 mM of NHS prepared in MES for an hour

followed by 3x wash with MES buffer. Qualitative and quantitative analysis of such surface modifications were obtained by characterization with optical, FTIR, and XPS measurements. Blank Mo surface has a surface oxide state thereby forming a Mo-O groups (Figure 10). DSP is an amine-reactive crosslinker which have affinity towards amino groups of antibodies. The thiol chemistry between Mo and Sulphur is evaluated through material characterization of DSP functionalized Mo surface. EDC is commonly used to react with carboxylic functional groups. The other reactive end is conjugated with NHS thereby forming an amine-reactive esters of carboxylate functional groups. Amino groups of the antibodies bind to the cross-linkers. NHS couples with EDC to form a stable intermediate ester functional group. The primary amines of the proteins react with the ester to form a stable amide conjugate.

Biosensing protocol

Surface functionalized Mo samples were first washed with PBS thrice before treatment with antibody to maintain the same pH. Antibody immobilization was achieved by treatment with 1 μg/ml of α-CRP in PBS for 15 minutes followed by wash with testing buffer. Then, aliquots of CRP antigen diluted in synthetic urine buffer were tested on antibody immobilized biosensor surface starting with lowest concentration. All samples were incubated for five minutes followed by 3x wash with buffer. Electrochemical measurements were taken at each step of immunoassay and sample volume was maintained at 30 μL.

Characterization

Atomic force microscopy: The morphology of as deposited Mo was characterized with Veeco Model 3100 Dimension V atomic probe microscope. Tapping mode antimony doped Silicon coated with Chrome and Cobalt tips were used for imaging.

Contact angle measurements: The degree of hydrophobicity of free and functionalized Mo samples were determined using goniometer (Ramĕ-hart Instruments Co, NJ, USA) based on sessile-drop method. Measurements were taken at five different locations on the same sample with a pure water droplet of ~ 1 mL and average of these five values were denoted as contact angle.

Fluorescence microscopy: The qualitative analysis of crosslinker functionalized Mo samples labelled with Rhodamine 123 were acquired with Zeiss AXIO Vert A1 microscope equipped with HAMATSU OCRA-flash4.0 camera using 20X magnification. Labelling was achieved by treating functionalized Mo samples with 1 mM Rhodamine 123 dissolved in ethanol for 30 minutes in dark. Fluorescence images were then obtained with excitation at 509 nm and emission was collected at 539 nm. This study is used to evaluate the surface coverage of crosslinkers in a qualitative way only.

ATR-FTIR measurements: The infrared spectra of surface functionalized Mo samples were recorded on a Nicolet iS50 FTIR spectrometer equipped with Ge Attenuated Total Reflectance (ATR) accessory and DLaTGS detector. All absorbance spectral measurements were obtained at a resolution of 4 cm^{-1} for 256 scans in the spectral range between 4000 cm^{-1} and 600 cm^{-1}. Air was used as reference background spectra.

XPS measurements: The surface composition of free Mo and surface functionalized Mo samples were evaluated using X-ray photoelectron spectroscopy measurements. The samples were

analysed using PHI Versa Probe II X-ray photoelectron spectrometer equipped with Al Kα monochromatic X-ray source and photoelectron take-off angle of 45°. Survey scans were performed with pass energy of 187.850 and 0.8 eV. High resolution spectra were obtained with an analyser of 23.5 eV at 0.2 eV. All binding energy (BE) values were referenced to the main C 1s peak at 284.6 eV. Curve fitting and peak analysis were performed to understand the type of chemical interaction between the crosslinker molecule and Mo electrode. The atomic concentrations of the observed elements were calculated based on their corresponding peak areas.

Electrochemical measurements: The electrochemical performance of Mo biosensor was evaluated using Ref 3000 potentiostat from Gamry instruments. Cyclic voltammetry measurements in presence of the $K_3Fe(CN)_6$ from -0.8 V to +0.8 V with a scan rate of 100 mV/s was performed to characterize electrode stability in various buffer medium. Similarly, EIS measurements were obtained by applying a perturbed AC voltage signal of 10 mV amplitude over frequency range from 1 Hz to 1 MHz under zero DC bias.

Results and Discussion

Surface morphology analysis

The mechanism that supports the covalent attachment of an organic molecule to sensor surface is its morphological characteristics. Several research groups in past have demonstrated that the surface roughness influence assembly of crosslinker molecules on its surface. [86] Thus, the surface topography of deposited Mo thin films was evaluated using AFM in tapping mode. As shown in Figure 10, the scanned surface image demonstrates a smooth and featureless surface with root mean square value of roughness at 9.51 nm on glass substrate. This result confirms the conformal

deposition of Mo on to glass substrate. The scanning electron microscope (SEM) image (Figure 10) indicated a uniform deposition of Mo on the flexible nanoporous polyamide substrate.

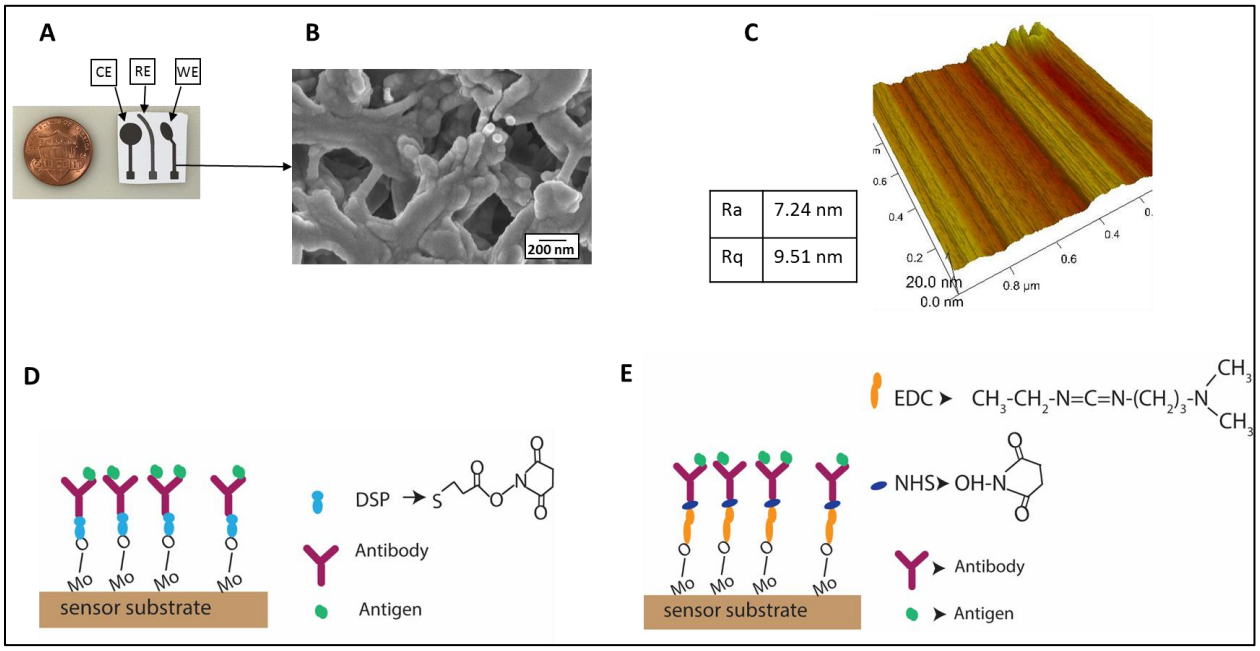

Figure 10. Molybdenum crosslinker binding chemistry

(A) Mo sensor indicating the three-electrode system. (B) SEM image of Mo deposited on a porous membrane substrate indicating uniform deposition. (C)AFM image of Mo surface indicating a smooth profile indicating a uniform deposition of Mo on the sensor substrate and the insert table indicating Ra(roughness average) and Rq(roughness root mean squared) (D) Schematic representation of binding between Mo surface with the native surface oxide layer and DSP cross-linker. (E) Schematic representation of binding between Mo surface with the native surface oxide layer and EDC-NHS cross-linker

Surface wettability is another characteristic that determines interaction of organic crosslinker molecules with Mo surface. Hence, contact angle measurements were conducted on free and

surface functionalized Mo samples on glass substrate and obtained results are shown in Figure 11. Mo thin films show hydrophilic nature with measured contact angle at 49 ± 6°. After treatment with DSP, contact angle of Mo was measured to be 32.1±2°. The contact angle of Mo surface after EDC-NHS functionalization was measured to be 45±2°. Such a decrease in wettability characteristics is evidence of assembly of organic functional groups on to Mo surface. In order to compare the efficiency of surface coverages of thiol and carbodiimide cross-linkers, we performed fluorescence microscopic characterization.

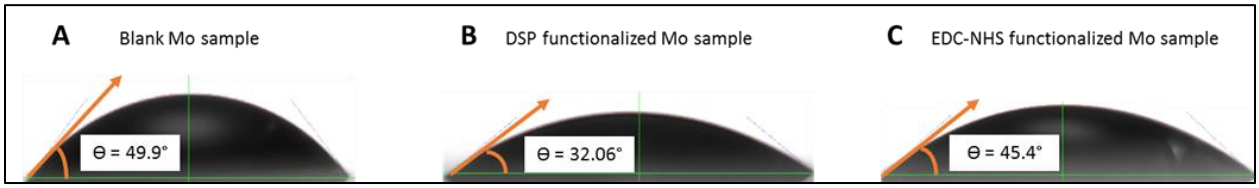

Figure 11. Contact angle measurements

Contact angle measurements on (A) Blank Mo sample. (B) DSP functionalized Mo surface (C) EDC-NHS functionalized Mo surface. The decrease in the contact angle measurements with respect to the blank Mo sample indicates the modification of surface

Fluorescence microscopy analysis

In order validate the success of Mo surface modification, we labelled the functionalized surface with a green fluorescent dye namely Rhodamine 123 and performed studies with fluorescence microscopy on Polyethylene terephthalate (PET) substrate. The NH_2 groups of this chemical compound specifically binds to NHS ester terminations in the crosslinker molecule and would fluoresce when excited at 509 nm. Figure 12 shows the fluorescence microscopy analysis of chemically modified Mo surfaces using fluorophore pre- and post-wash. In general, Mo due to its high electrocatalytic properties has tendency to adsorb organic molecules on to its surface. This

behaviour poses an important challenge for accurate determination of effective surface coverage via covalent attachment either via physisorption or chemisorption. Hence, these experiments involved a blank Mo surface treated with fluorophore molecule as a control.

Figure 12 shows high-background signal caused by presence of high concentration of fluorophore on Mo surface prior to wash step. We performed 5x wash with DI water to remove unbound Rhodamine 123 molecules as it has the potential to interfere with qualitative determination of surface coverage by crosslinker molecules. After washing, the fluorescence observed is evident of crosslinker molecules binding to Mo surface and Figure 12 represents the images acquired on free, DSP and EDC-NHS functionalized Mo surface. Higher the observed fluorescence, higher is the density of tested crosslinker on Mo surface. EDC-NHS shows better coverage than DSP indicating dominant functionalization of carboxylic acid groups on to Mo surface. However, these results represent the effective number of linker molecules attached on to Mo surface only, while no information regarding surface composition and chemistry is available.

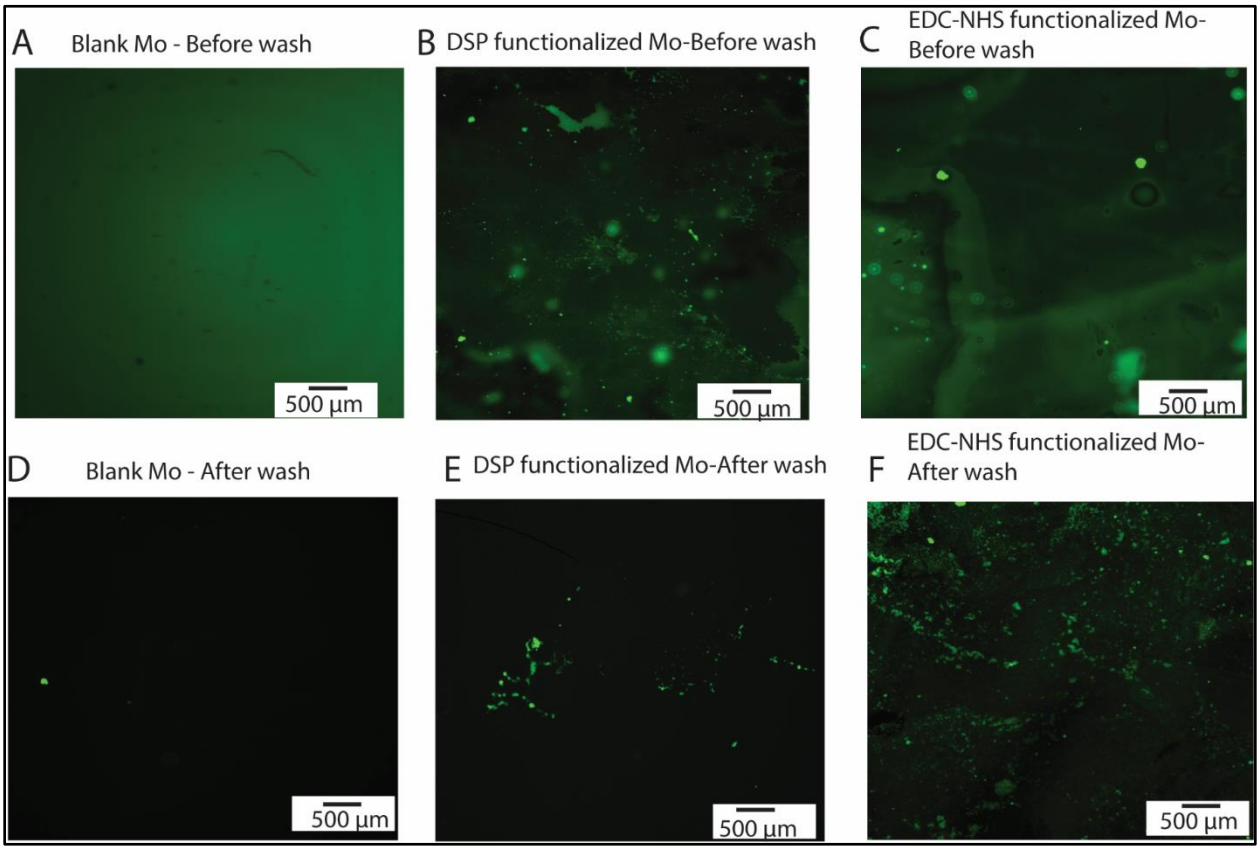

Figure 12. Optical characterization of binding of Fluorescent molecule 123

(A) Blank Mo surface before wash condition (B) DSP functionalized Mo surface before wash condition(C) EDC-NHS functionalized Mo surface before wash condition (D) Blank Mo surface after wash condition (E) DSP functionalized Mo surface after wash condition indicating surface coverage of Rh123 thereby indicating binding of DSP cross-linker on Mo surface (F) EDC-NHS functionalized Mo surface after wash condition indicating enhanced surface coverage of Rh123 thereby indicating better binding of EDC-NHS cross-linker on Mo surface

ATR-FTIR analysis of surface modified Mo

The formation of Mo-linker binding and the subsequent chemical interactions was investigated using ATR-FTIR measurements on glass substrate. The appearance of dominant peak corresponding to molybdenum oxide represents the native oxide layer on Mo sample. Figure 13 illustrates the baseline corrected absorbance IR spectra of Mo surfaces after functionalization with crosslinker molecules in order to enhance the resolution of peaks resulting from the chemical interaction of cross-linkers with Mo sample. Under all conditions, IR spectra displays a broad and dominant peak in the range between 800 cm^{-1} and 1000 cm^{-1}, which is indicative of terminal metal-oxygen bonds.[87] Appearance of oxide peaks (i.e. Mo=O stretch) in the spectra is attributed to be from passive oxide layer formation on deposited Mo thin films. The FTIR spectra of DSP functionalized Mo sample after subtraction of Mo spectra shows the peaks corresponding to organic functional groups (Figure 13 A). The peak at 1718 cm^{-1} corresponds to the presence of ν(C=O) functional groups.[88] The appearance of a peak at 2895 cm^{-1} corresponds to the presence of ν (CH_2) functional groups.[89] The appearance of weak peaks corresponding to these organic functional groups indicate the possible chemical interaction of DSP cross-linker onto the Mo sample.

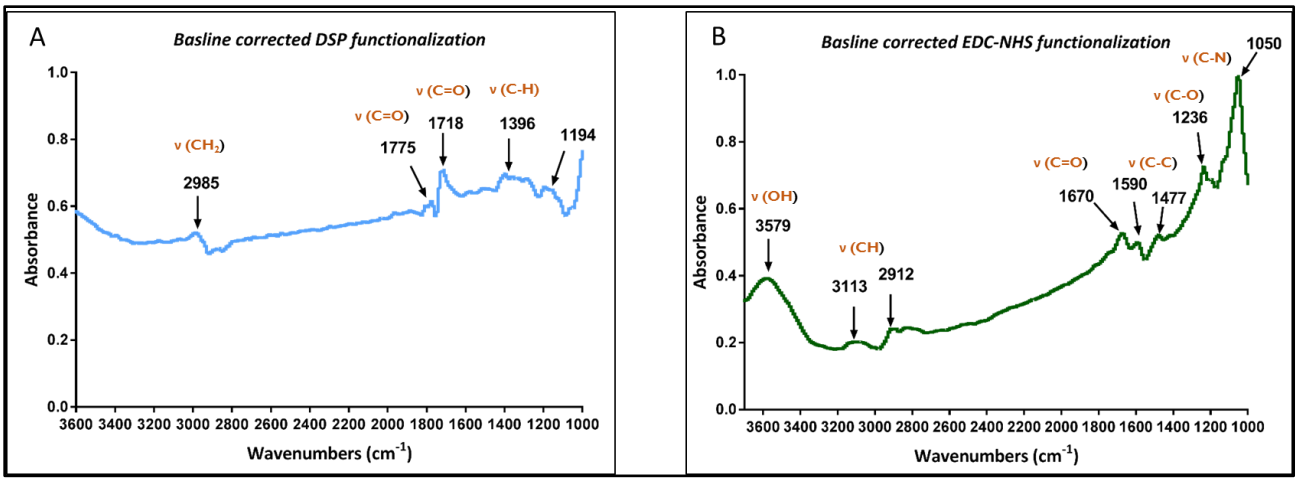

Figure 13. FTIR characterization on crosslinker functionalization

(A) FTIR spectra of DSP functionalized Mo sample after subtraction of the baseline Mo spectral peaks. (B) FTIR spectra of EDC-NHS functionalized Mo sample after subtraction of Mo spectral peaks. The spectra indicate the occurrence of peaks corresponding to organic functional groups which indicate the possible chemical interaction between the cross-linkers with Mo sample.

The blank corrected FTIR spectra of EDC-NHS functionalized Mo sample is shown in Figure 13B. The peaks corresponding to blank Mo sample were subtracted from the FTIR spectra and analysed for EDC-NHS specific peaks. The spectra indicate a dominant peak at 3579 cm^{-1} which corresponds to the (OH) stretch in a carboxylic acid functional group.[90] The peak at 2840 cm^{-1} corresponds to the stretching of (C-H) bond in alkyl functional groups.[91] The occurrence of peak at 1670 cm^{-1} corresponds to the stretching vibration of ν(C=O) amide functional groups.[92] The peak occurrence at 1050 cm^{-1} is attributed to stretching of ν(C-N) bonds of aliphatic amines.[93]

However, IR spectra of both these crosslinker functionalization shows no other characteristic peaks that corresponds to chemical structure of the molecule. This might be because the absorbance intensity of other peaks is diminished by very high intensity from oxide peaks and hence no

significant changes are observed in the IR spectra. The appearance of more relevant signature peaks corresponding to the carbodiimide cross-linkers indicate semi-quantitatively that EDC-NHS may have a better chemical binding interactions with Mo surface as compared to DSP cross-linkers.

XPS analysis of surface modified Mo

The chemical states of elements in a surface-functionalized Mo samples were investigated through XPS peak analysis. The XPS experiments were performed with Mo deposited on a glass substrate. For all conditions, recorded Mo 3d core level spectrum shows a doublet that is associated with Mo $3d_{3/2}$ and Mo $3d_{5/2}$ spin orbit coupling. Deconvolution and peak fitting with Gaussian function shows that core levels of 3d spectrum can be fitted with two separate groups of Mo 3d doublets, which corresponds to different oxidation states. The binding energies are represented in Table 2. Spectra consisted of Mo $3d_{5/2}$ binding energies at 228.81 eV and 229.69 eV, 228.21 eV and 229.16 eV and 227.51 eV and 228.47 eV for free Mo, DSP treated Mo and EDC-NHS treated Mo respectively. Peak positions for Mo $3d_{3/2}$ were at 231.87 eV and 232.42 eV surfaces. These peak positions are in agreement with those found in literature for metallic Mo and various oxidation states (i.e. Mo^{+5} and Mo^{+6}).[94]

The O 1s spectrum shown in Figure 14A displays existence of two peaks each for Mo and DSP treated Mo. The peak observed at ~ 530 eV is attributed to oxide formation and peak at ~532 eV is due to adsorbed oxygen on to Mo.

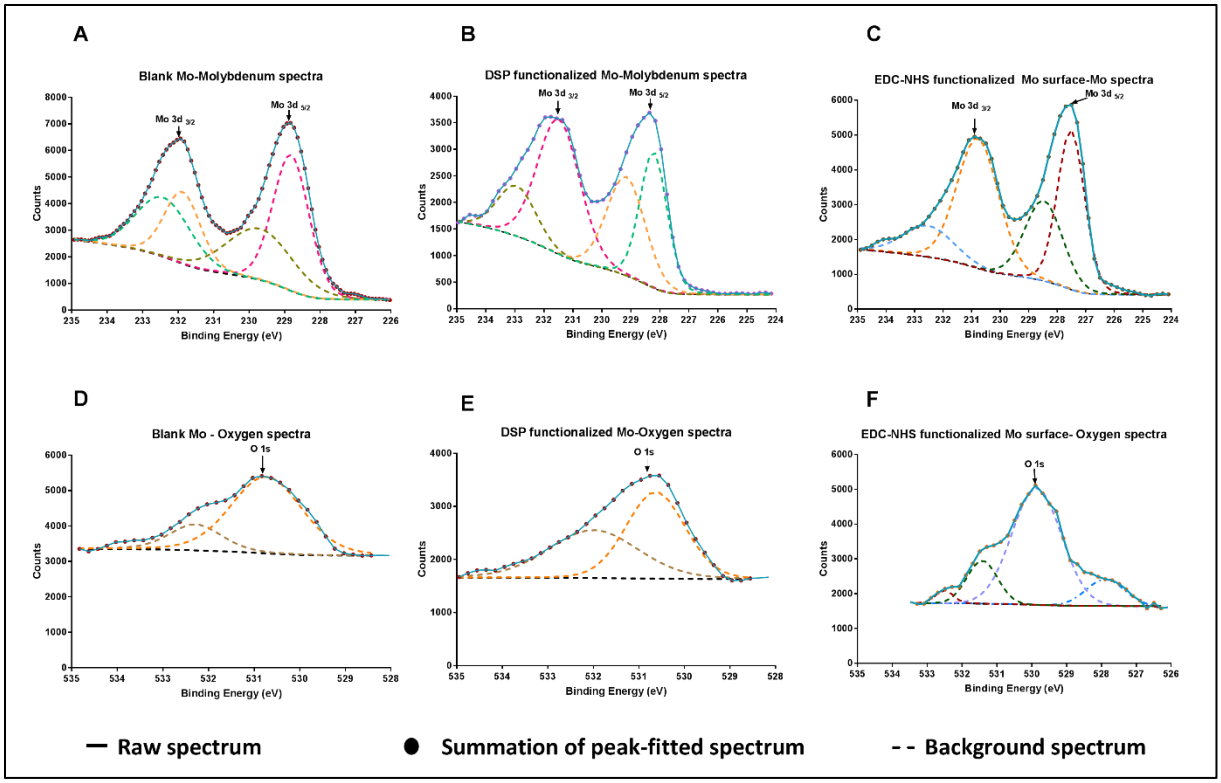

Figure 14. XPS spectra on molybdenum and oxygen

(A) XPS spectra of blank molybdenum indicating doublet 3d peaks (B) XPS spectra of DSP functionalized Mo (C) EDC-NHS functionalized Mo sample (D) Oxygen 1s XPS spectra of blank Mo sample (E) Oxygen 1s XPS spectra of DSP functionalized Mo sample (F) Oxygen 1s XPS spectra of EDC-NHS functionalized Mo sample

The chemical states of Mo, DSP treated Mo and EDC-NHS treated Mo were investigated by XPS for Mo, at 231.49 and 232.94 eV for DSP treated Mo and at 230.78 eV and 232.53 eV for EDC-NHS treated Mo to confirm surface modification both qualitatively and quantitatively.

For all conditions, recorded Mo 3d core level spectrum shows a doublet that is associated with Mo $3d_{3/2}$ and Mo $3d_{5/2}$ spin orbit coupling (Figure 14). Deconvolution and peak fitting with Gaussian function shows that core levels of 3d spectrum can be fitted with two separate groups of Mo 3d

doublets, which corresponds to different oxidation states. In the case of EDC-NHS treated Mo, decomposition of core O 1s spectrum shows existence of four peaks with binding energies at 527.89 eV, 529.86 eV, 531.42 eV and 532.50 eV. The major peak at observed at 531.42 eV is due to the presence of organic C-O bonds which is evidence of functionalization of Mo surfaces with EDC-NHS.

Analysis of C 1s spectrum is shown in Figure 15. The most noticeable peak at ~284.8 eV is attributed to presence of C-C bonds due to carbon contamination or from functionalized crosslinker molecules. We observe two additional peaks at 286.27 eV and 288.45 eV which are due to presence of organic C-O-C and O-C=O bonds in EDC-NHS treated Mo surfaces.

Similarly, decomposition of N 1s spectrum for all the three conditions is represented in Figure 15**.** The peak observed at a binding energy of ~395.7 eV is characteristic of Mo $3p_{3/2}$ component while those observed at lower binding energies i.e. ~394 eV is attributed to Mo 3p. EDC-NHS treated Mo displays a peak at ~399 eV that is attributed to imide nitrogen in the crosslinker molecule. This further confirms the covalent attachment of EDC-NHS to Mo surface. We also observe a weak shoulder at a binding energy of ~397 eV which is in agreement with literature for metallic nitrides and much more detail studies have to be conducted to confirm this peak assignment.[95]

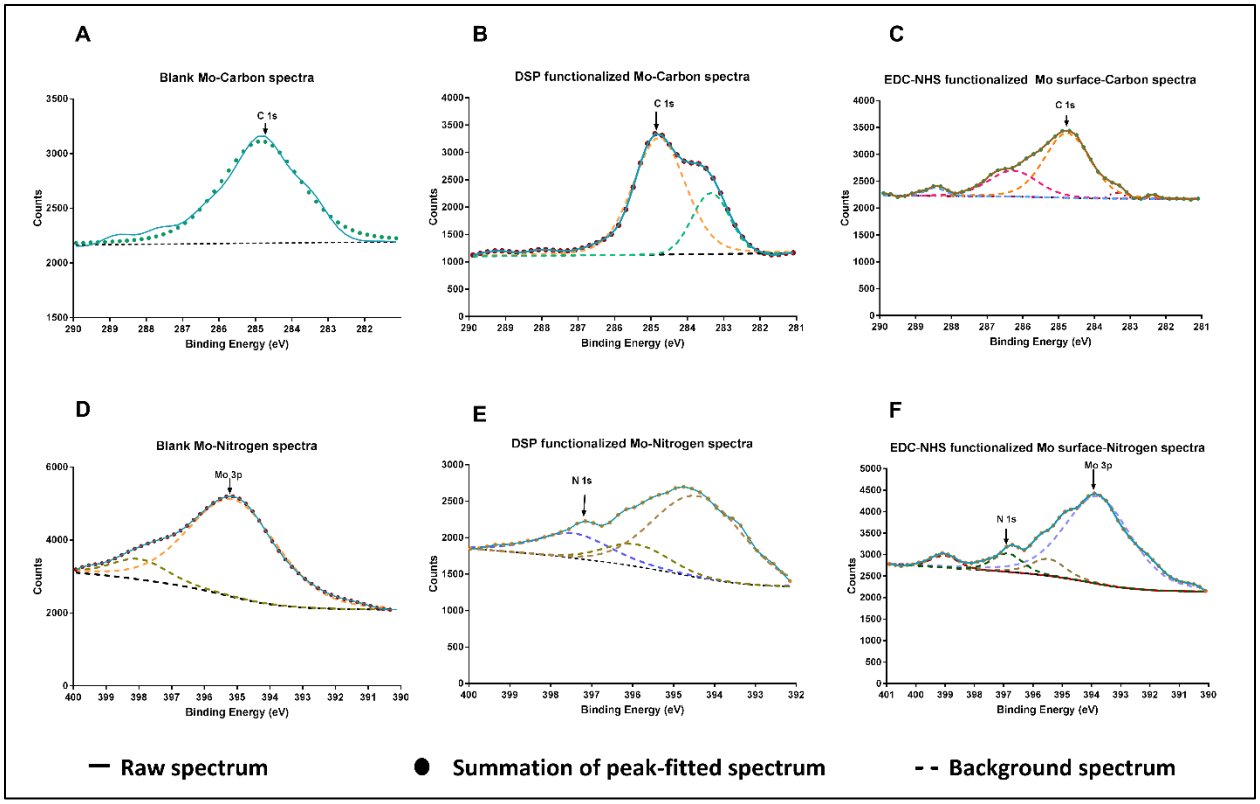

Figure 15. XPS spectra of Carbon and Nitrogen

(A) XPS spectra of Carbon 1 s spectra of blank Mo (B) XPS spectra of Carbon 1s of DSP functionalized Mo sample (C) XPS Carbon 1s spectra of EDC-NHS functionalized Mo sample. (D) XPS spectra of Nitrogen in blank Mo. (E) XPS spectra of Nitrogen 1s in DSP functionalized Mo (F) XPS spectra of Nitrogen 1s of EDC-NHS functionalized Mo sample

Table 2. Comparison of position of Mo peaks in cross-linker in cross-linker functionalized samples

Sample Type	**Binding Energy (eV)**			
	Mo $3d_{3/2}$		Mo $3d_{5/2}$	
Blank Mo	231.87	232.42	228.81	229.69
Mo+DSP	231.49	232.94	228.21	229.16
Mo+EDC-NHS	227.51	228.47	230.78	232.53

Thus, the high-resolution chemical studies conducted on different Mo surfaces reveal successful functionalization of Mo with carboxylic acid functional groups and very weak binding interactions with thiol groups.

Electrochemical characterization towards proof-of-feasibility for urinary biomarker analysis.

The ionic properties of the buffer affect the electrochemical performance of the electrode. The comparison of pH values of the buffers is demonstrated in Figure 16A. The pH of synthetic urine was measured to be slightly acidic when compared to other buffers. The effect of the ionic properties of the buffer on the electrochemical performance of electrode was evaluated through cyclic voltametric studies (Figure 16B). The baseline electrochemical characterization studies were performed on glass substrate. The positive voltage sweep demonstrated a positive electrochemical peak current of 30 μA at 0.25 V and a negative peak current of 20 μA at 0.2 V. These electrochemical peaks are attributed to the presence of Mo^{3+} and Mo^{6+} species.[5] The data is plotted is the mean value obtained from three cycles of measurement. The open circuit potential (OCP) of all the buffers reached a steady state within 10 minutes and maintained stability after reaching steady state (Figure 16C). The steady state behaviour of Mo electrode for multiple buffers

of varied pH indicate the ability of Mo for use in dipstick based electrochemical diagnostic biosensors.

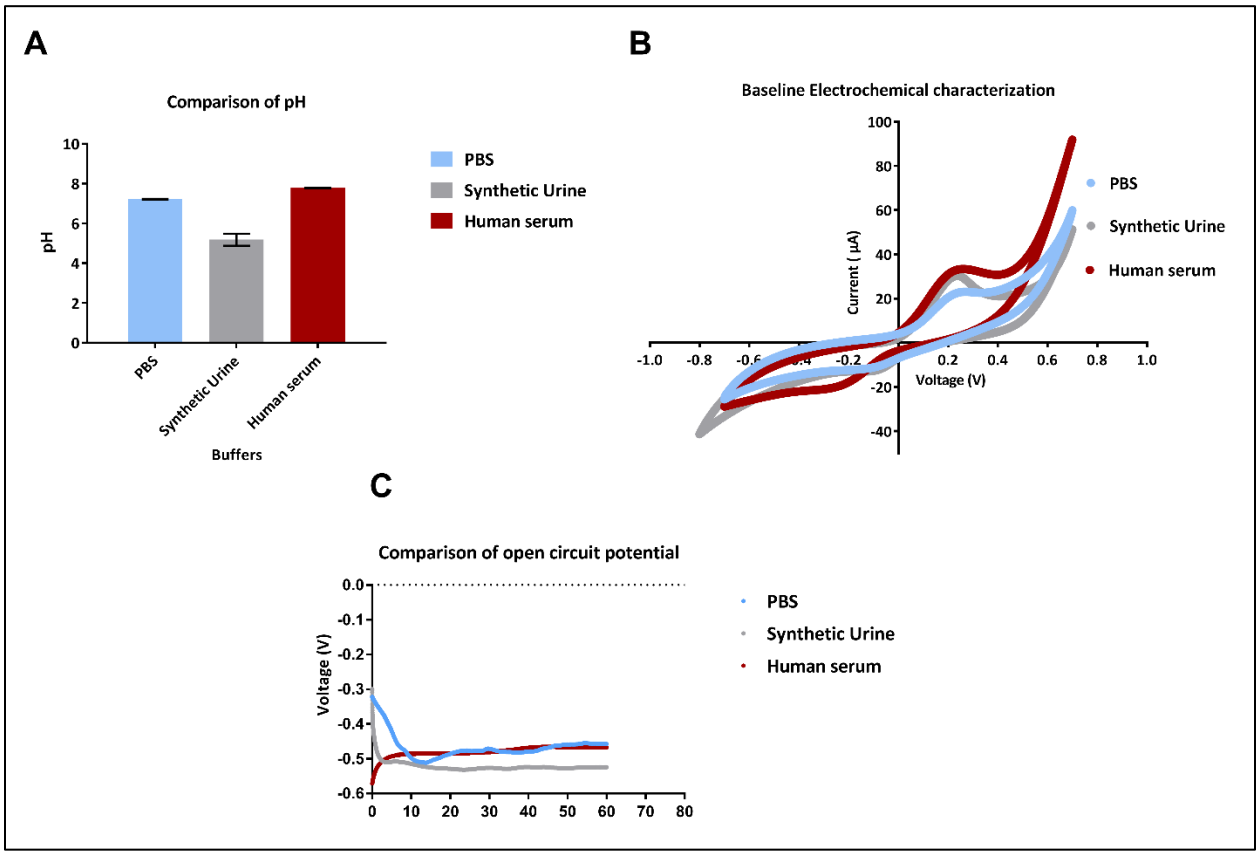

Figure 16. Electrochemical characterization of molybdenum electrode

(A) Comparison of pH for multiple buffers spanning acidic, neutral and alkaline media. Error bars indicate standard error of mean from N=3 replicates. (B) Evaluation of electrochemical properties with cyclic voltammetry experiments for multiple buffers. (C) Estimation of time to steady state for buffer media indicating that the electrode reaching steady state within 10 minutes for all the tested buffers

Affinity based biosensing was demonstrated using CRP protein with non-faradaic EIS method on nanoporous polyamide substrate. Binding interactions between the surface-functionalized anti-

CRP antibody and the CRP antigen biomolecules results in the formation of electrical double layer at the interface of electrode and buffer electrolyte. In an Impedimetric based assay, these binding interactions at the electrical double layer causes changes in the impedance. The changes in impedance is associated with resistive and capacitive components. The dominant resistive components are solution resistance (R_s) and charge transfer resistance (R_{ct}). The biomolecular binding causes a transient build-up of charges which results in the changes in the capacitance. The changes in double layer capacitance (C_{dl}) is the major capacitive component affecting the changes in impedance. Nyquist and Bode plot analysis were performed to evaluate the electrochemical performance of the biosensor (Figure 17). Nyquist analysis indicated that a clear distinguishability between the multiple CRP concentration. The effect of buffer's ionic properties is attributed to changes in solution resistance which is observed at higher frequencies (>1000 Hz). Bode phase plot indicated maximum changes in phase at lower frequencies. The demonstration of changes in the phase of impedance is attributed to capacitive changes which thereby indicate the binding of biomolecules. Maximum capacitive changes in phase were observed at 10 Hz (Figure 17B). The calibration dose response (CDR) curve was henceforth plotted at 10 Hz frequency (Figure 17D). Clear distinguishability in the CRP dose concentrations from 100 pg/ml to 1 µg/ml were obtained. The sensor was tested in synthetic urine buffer medium. The Z_{mod} measured at blank dose without antigen was measured to be 32 kΩ. The sensor demonstrated a higher change in impedance with increase in the CRP antigen concentrations. A 34% change in impedance with respect to blank buffer for the lowest detectable CRP concentration of 100 pg/ml was measured. The change in impedance with respect to blank buffer was calculated to be 75% for the highest concentration of 1 µg/ml. The higher change in impedance is the result of increase in the capacitance developed

due to biomolecular binding. The experimental values were fitted to the equivalent Randles electrical circuit as shown in Figure 17 C. The experimental fit results indicated an increasing trend for double layer capacitance (C_{dl}) for increasing CRP antigen concentrations (Table 3). The resistive R_{ct} component did not change appreciably for multiple CRP concentrations thereby indicating that the change in impedances are driven by capacitive components in the circuit. The other electrical parameters of the sensor were attributed to the resistance (R_{Mo}) and capacitance (C_{Mo}) of molybdenum. However, these parameters did not change as a correlation to protein concentrations. Thus, the linear correlation between changes in impedance with increasing CRP concentrations indicates efficient binding interactions of biomolecules on the Mo electrode.

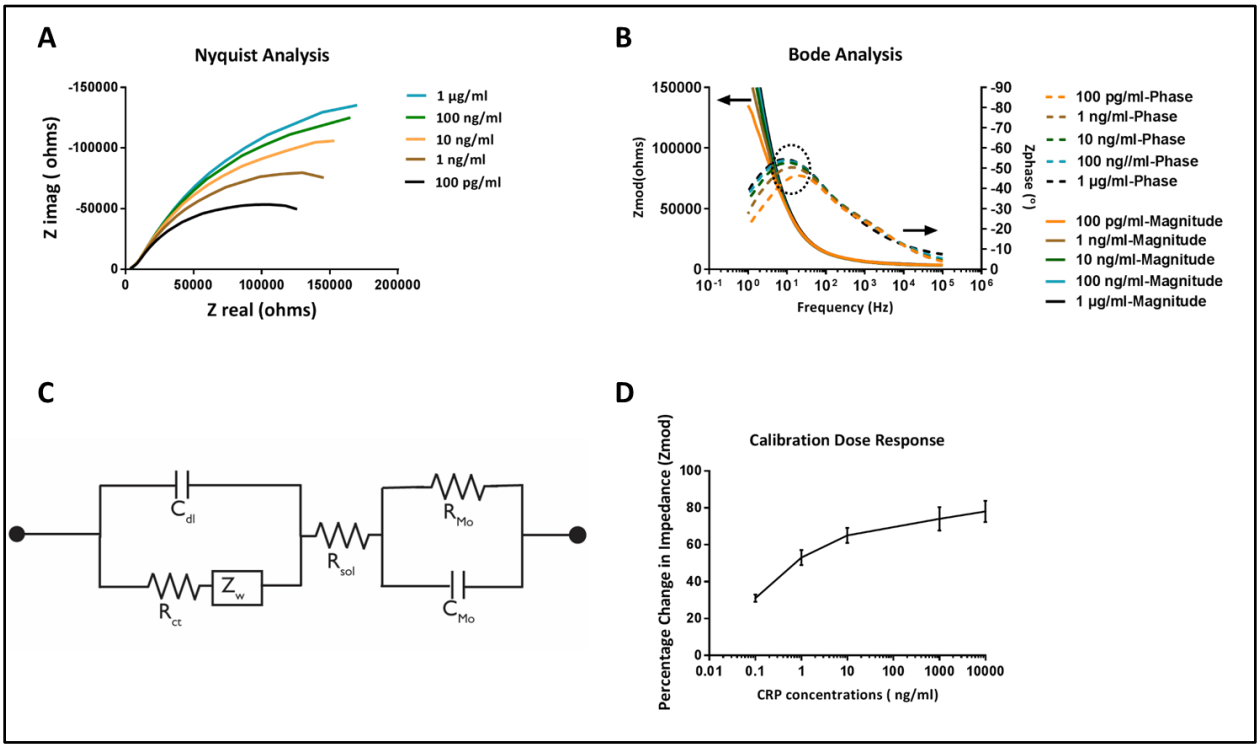

Figure 17. EIS characterization for CRP detection

(A) Nyquist plot indicating distinguishability between multiple CRP antigen concentrations (B) Bode magnitude and phase analysis indicating maximum capacitive phase changes at encircled

region at 10 Hz. (C) Equivalent electrical circuit diagram of Mo biosensor (D) Calibration dose response curve indicating percentage change in impedance for multiple CRP concentrations. Error bars indicate standard error of mean from N=3 replicates

Table 3. Estimation of experimental data-fit parameters

Estimation of data-fit parameters		
CRP concentration	**R_{ct} (ohms)**	**C_{dl} (F)**
100 pg/ml	87521	6.24E-07
1 ng/ml	87600	6.74E-07
10 ng/ml	87611	7.18E-07
100 ng/ml	87609	7.37E-07
1 µg/ml	87597	7.85E-07

Conclusion

In summary, the binding interactions between Mo electrode and two cross-linker molecules namely DSP and EDC-NHS have been characterized. The XPS and FTIR characterization results showed evidence of binding of cross-linker molecules to the Mo electrode in spite of the presence of passive oxide layer. EDC-NHS cross-linker was favourable over DSP for binding to Mo electrode surface. Electrochemical characterization of Mo electrode demonstrated the stability of Mo electrode for different buffer solutions. Affinity based electrochemical biosensing application of Mo electrode was demonstrated using EIS method. The impedance of the sensor showed an increasing trend in change in impedance with increase in the CRP antigen concentration. A limit of detection threshold of 100 pg/ml was achieved in synthetic urine buffer. This concentration is

also the physiological threshold concentration for elevated presence of CRP in urine.[85] The stable behaviour of Mo electrode in multiple buffer media may be utilized to develop dipstick based biosensors.

CHAPTER 6

PORTABLE ELECTROCHEMICAL DIPSTICK BIOSENSOR USING MOLYBDENUM ELECTRODE FOR DETECTION OF INFLMMATORY BIOMARKERS

Abstract

Molybdenum (Mo) electrode has been used to develop electrochemical dipstick biosensor for the detection of two key inflammatory biomarkers, CRP and IL-6. Non-faradaic, label-free Electrochemical Impedance Spectroscopy (EIS) was used to capture the signal response occurring from biomolecular binding. Binding affinity between EDC-NHS crosslinker and antibodies on Mo surface was validated through Fourier Transform Infrared Spectroscopy (FTIR) technique. The sensor's performance was evaluated in human urine samples and synthetic urine of three pH ranges (5.5, 6.5 and 7.5). The scope for portability in the design was demonstrated by preliminary comparison of impedance measurements between standard potentiostat and portable hardware prototype.

Introduction

Inflammatory biomarkers are significant predicators of physiological condition in humans. Two prominent markers in particular, CRP and IL-6, are associated with various disease conditions such as cardiovascular disease, depression, renal insufficiency, cancer, Chronic Obstructive Pulmonary Disease (COPD) etc.[96] Elevated levels of the cytokine IL-6 has also been associated with various types of cancers, periodontal disease, arthritis, as well as type-2 diabetes. The detection of IL-6 in urine holds critical significance in the diagnosis of urinary infections. Elevated

levels of IL-6 has been observed in cases of patients who had undergone kidney transplantation and in acute rejection situations.[97] The levels of IL-6 in patients diagnosed with asymptomatic bacteriuria has been found to be present at an elevated levels only in urine and not in serum citing local production of IL-6.[98] Thus, IL-6 detection in urine holds relevance in such local occurrence of elevated levels in cases of renal diseases. C-reactive protein (CRP) is a significant biomarker for diagnosis of inflammatory responses. During inflammatory stimulus, the CRP levels show a significant spike in its levels. Table 4 summarizes the past work towards detection of biomolecules in urine. Majority of the prior work have focused on the detection of metabolites in the urine. Early detection of elevated levels of these biomarkers would help to prevent mortality due to fatal diseases. In isolation, elevated levels of these biomarkers could lend themselves to a vast range of differing diagnosis, but in conjunction with detection of other biomarkers a greater level of granularity can be achieved in the resulting diagnosis. Thus, the development of a point-of-care (PoC) diagnostic biosensor for the detection of inflammatory disease has great value towards reliable home-based monitoring of diseases.

The emergence of PoC diagnostic biosensors has enabled the early detection of disease, reducing diagnosis time requirements compared to reliance on laboratory based testing. The cost-effectiveness and rapid detection features of these PoC biosensors has made them attractive for use in resource limited environments for rapid disease diagnosis.[99] Thus, diagnostic utility of PoC biosensors for the detection of biomarkers from physiological media such as sweat, urine, and saliva has been of significant interest owing to their non-invasive mechanism of detection. There is no necessity for trained personnel to collect specimens thereby enabling home based disease diagnosis.[27] The class of dipstick based biosensors have been demonstrated for rapid biomarker

detection.[100] Easy manufacturability and user-friendly design of the dipstick form factor has favored their use in pH strips as well as several urine dipstick test kits.[34, 100a] The output format of the current dipstick biosensors are predominantly qualitative and colorimetric in nature which makes integration with other data readout devices challenging.[101] Thus, there is an imminent need for biosensors which can provide quantitative or semi-quantitative information about the target analyte. Unlike their colorimetric counterpart, electrochemical dipsticks help in addressing the challenges associated with visual interpretation of results and also favors the miniaturization of form-factor.[102] Electrochemical dipsticks provide quantitative/semi-quantitative output and can be interfaced with other electronic indicator hardware. They also have scope for miniaturization and are inexpensive as they possess scope for large scale manufacturing. The development of dipstick biosensors is focused on the non-invasive based detection of biomarkers from biological fluids such as urine, sweat, saliva etc. Urine is considered a useful biological fluid as it consists of a mixture of many significant proteins which are of relevance for disease diagnosis. Urinary concentrations of inflammatory biomarkers such as IL-6 and CRP are elevated during disease conditions.

Table 4. Prior work on urine based biomolecule detection

Class	**Biomarker**	**Detection Method**	**Detection Limit**	**Response Time**	**Reference**
Metabolite	Glucose	Colorimetric	3e-7 mol L^{-1}	20 minutes	[103]
	Human serum Albumin (HSA)	Chemiluminescence	2.5 mg L^{-1}	32 minutes	[104]
	Cocaine	Colorimetric	1 nM	N/A	[105]
	Human growth hormone (hGH)	Bimodal Waveguide Interferometry	10 pg mL^{-1}	8 minutes	[106]
	Creatinine	Electrochemical	16 pg/mL	N/A	[107]
Bacteria	S. haematobium	Electrochemical	0.53 ng/μL	60 minutes	[108]
Protein	NMP22	Electrochemical	3.3 pg/mL	N/A	[109]
	hCG	Electrochemical	2.4 pg/mL	30 minutes	[110]
	TGF-β1	Electrochemical	10 pg/mL	20 minutes	[111]
	IL-6 , CRP	Electrochemical	1 pg/mL	5 minutes	This work

The development of flexible substrate based biosensors enable the development of disposable point of care biosensors which can be manufactured in large batches in a cost-efficient manner. Various flexible porous substrates have been evaluated as biosensor substrates owing to their ability for large scale batch manufacturing and disposable nature.[112] These nanoporous substrates also aid in the amplification of signal response from affinity based binding of biomolecules in the

pores. The presence of nanoporous structures enhance the charge screening from non-specific molecules.[24] Polyamide membranes are a favorable biosensor substrate due to their physical stability and hydrophilic property making them ideal candidates for a dipstick assay. Electrodes can be easily deposited on to the flexible polyamide membrane through various metal deposition technique. The electrochemical properties of the electrode material are the driving factor in capturing the signal response from the biomolecular binding. In the past, Gold has been the preferred choice of electrode material for various electrochemical biosensors. However, there is a growing research in the evaluation of other transition group elements as biosensor electrodes. Molybdenum is a transition group element and its compounds have demonstrated good electrical conducting properties.[113] The compounds of molybdenum have been evaluated as cathode for lithium batteries.[114] Molybdenum oxide films exhibit pseudocapacitive property which has favored its use as electrode material in micro-scale electrochemical capacitors due to enhanced charge storage kinetics.[115] Pseudocapacitance is a phenomenon of charge storage at or near the surface of the material.[116] Molybdenum oxide has been evaluated as an electrode material in Lithium ion batteries due to their favorable electrochemical properties.[117] Thus, the favorable electrochemical properties of Mo support their evaluation as an electrode material for electrochemical biosensors. This work is focused on the development of portable point of care dipstick biosensor for multiplexed detection of IL-6 and CRP in human urine using non-faradaic Electrochemical Impedance Spectroscopy (EIS) biosensing. Mo forms a passive surface oxide layer which restricts the choice of crosslinkers to those which exhibit affinity to metal oxide chemical species. EDC-NHS is one such crosslinker which has been evaluated for chemical conjugation with metal oxide thin films.[118] The binding interactions between EDC-NHS functionalized Mo and CRP and IL-6

antibody have been characterized through Fourier Transform Infrared Spectroscopy (FTIR). The detection of CRP and IL-6 in human urine and synthetic urine has been demonstrated using non-faradaic EIS technique covering the physiologically relevant ranges of pH.

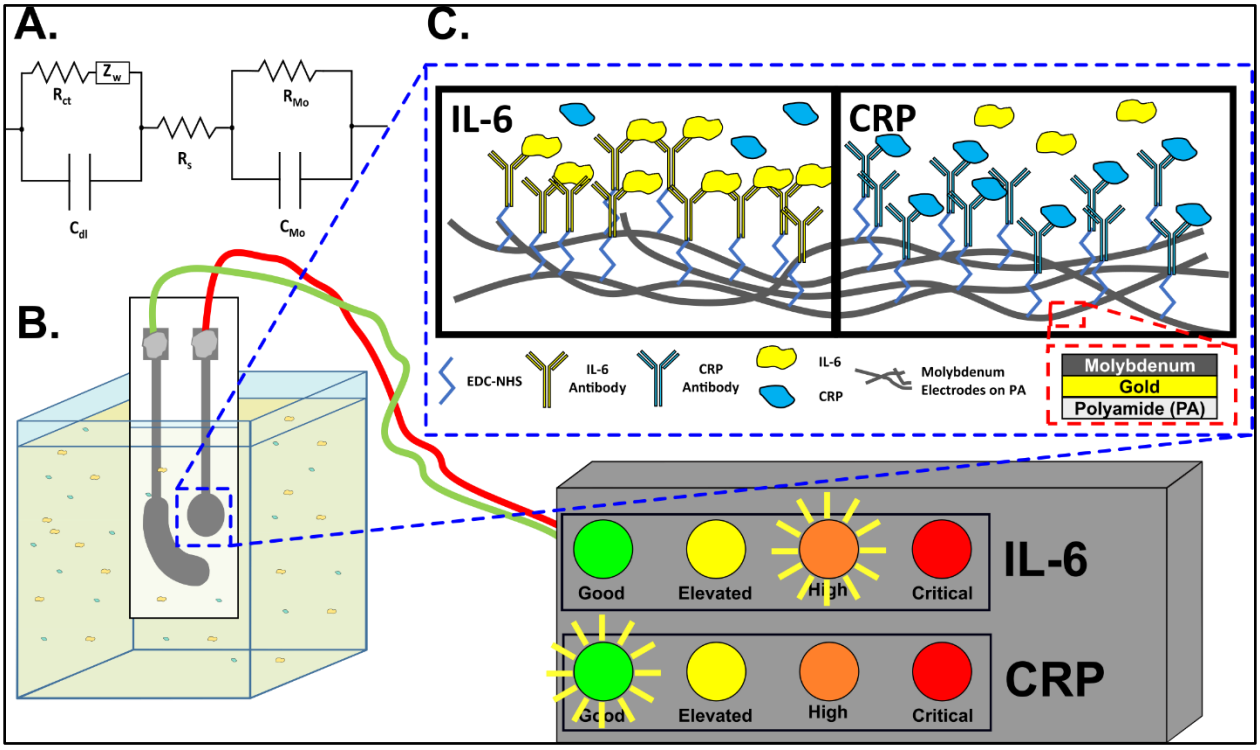

Figure 18. Schematic representation of dipstick biosensor

A) Modified Randles Cell used to model the molybdenum sensor interface. **B)** Schematic representation of the sensor, experimental set-up, and device display. **C)** Schematic detailing the constructed assay for both detection of IL-6 and CRP.

Materials and Methods

Materials and Reagents

N-hydroxysuccinimide (NHS), 1-ethyl-3-(3-dimethylaminopropyl) carbodiimide hydrochloride (EDC), 2-(N-Morpholino)ethanesulfonic acid (MES, pH 3), phosphate buffered saline (PBS, 0.1 M, pH 7), were obtained from Sigma Aldrich (MO, USA). α-CRP antibody, α-IL-6 antibody and CRP antigen were procured from Abcam (MA, USA). IL-6 protein was procured from Thermo Fisher Scientific Inc. (MA, USA). Pooled human urine samples were purchased from Lee Biosolutions, Inc (MO, USA) Acrylic cellulose acetate sheets were obtained from Staples (TX, USA). Kapton backing support material was obtained from McMaster Carr (TX, USA). Polyamide membranes of 200 nm pore size were obtained from GE Healthcare (NJ, USA) All solvents and reagents were of analytical grade and used as received.

Fabrication and assembly of Mo biosensor

The two-electrode pattern utilized in this work was designed in Autodesk AutoCAD software and was translated to the base polyamide substrates using acrylic cellulose acetate shadow masks during electron beam evaporation process. Gold was deposited as the base layer to improve the overall sensor conductivity. Molybdenum was deposited upon the gold base layer leaving the contact pads exposed for interfacing with instruments. Post deposition, the sensors were stored under nitrogen desiccation until use. To give the dipstick sensor structural integrity a Kapton adhesive backing was affixed to the bottom of the fabricated sensor. A secondary acrylic adhesive glue was patterned just below the contact pads of the sensor to restrict the samples ability of wicking to, and shorting the electrical contact pads.

Experimental protocol for biosensing experiments with synthetic urine

A 1:1 mixture of 100 mM N-hydroxysuccinimide(NHS) and 400 mM 1-ethyl-3-(3-dimethylaminopropyl) carbodiimide hydrochloride (EDC) was dissolved in 2-(N-Morpholino) ethanesulfonic acid (MES, pH 3) buffer just prior to the incubation. EDC-NHS mixture was immediately introduced at the sensing region of the sensor and incubated for one hour. EIS measurements were performed at each assay functionalization and dose step on the lab instrument and constructed instrumentation in parallel, using a Gamry Reference 3000 potentiostat (PA, USA) as the lab instrument. An alternating current (AC) voltage of 10 mVRMS was applied with a frequency sweep of 1 Hz to 1 MHz. Post EDC-NHS functionalization, 8 µL of PBS was added to the sensing region to remove any unbound crosslinker. 10 µg/ml of monoclonal antibody (IL-6 /CRP) in 0.1 M PBS was added and incubated for 15 minutes. A zero dose or blank dose measurement was performed by dipping the sensor in a cuvette containing synthetic urine in the absence of CRP or IL-6.The sample volume of the buffer in the cuvette was maintained at 300 µL. Three different pH ranges (5.5, 6.5 and 7.5) of synthetic urine buffer were tested for detection of CRP and IL-6. After a zero-dose baseline, the sensor was dipped serially in logarithmically increasing doses of target protein suspended in human urine allowing for a 5-minute incubation time before each measurement. A low IL-6 concentration of 1 pg/mL and a high concentration of 10 ng/ml was tested for each pH range of synthetic urine. All antigen doses were prepared in separate cuvettes. All doses were performed on a single sensor, but only one target protein was tested on any given sensor.

Experimental protocol for biosensing experiments with human urine

Electrochemical detection of the IL-6 and CRP were also performed with pooled human urine samples. The experimental protocol for the functionalization of crosslinker and antibody on Mo electrode was same as that of synthetic urine. IL-6 antigen concentrations from 1 pg/ml to 10 ng/ml and CRP antigen concentrations from 1 pg/ml to 100 ng/ml were tested with human urine.

FTIR characterization analysis

Attenuated total reflectance Fourier transform infrared (ATR-FTIR) spectrograms were obtained to establish the binding of the EDC-NHS crosslinker to the molybdenum surface, and subsequent binding of IL-6 and CRP antibody to the EDC-NHS crosslinker. The tool was equipped with a deuterated triglycine sulfate (DTGS) detector and KBr window. A Harrick VariGATR sampling stage with a 65° Germanium ATR crystal was used in this study. Measurements were taken in the range of 4000 – 600 cm^{-1} with 4 cm^{-1} resolution. Represented data is the average of 512 scans. ATR-FTIR samples were prepared as follows: Cleaned microscope slides were patterned with a layer of 100 nm Gold and 100 nm molybdenum using electron-beam evaporation process analogous to that used in the fabrication of the sensors. The bare molybdenum samples were sonicated with isopropyl alcohol and DI water and nitrogen dried completely before measurement. The functionalized samples were incubated with 100 µL of the EDC-NHS mixture for one hour. A 3x PBS wash was conducted to remove any unbound crosslinker. After washing and complete nitrogen dry, the Mo-EDC-NHS measurement was taken. After EDC-NHS functionalization, 100 µL of 10 µg/mL target antibody was incubated on the sample surface for an additional 30 minutes. A 3x PBS wash was conducted to remove unbound antibody. After a complete nitrogen dry the

antibody measurement was taken. All measurements represent individual samples. Samples were not used for more than one measurement.

Testing with portable electronic platform

The proof-of-concept portable electronic platform was built using off-shelf components and Arduino Uno R3 microcontroller. A digital-to-analog Converter in conjunction with a high-pass filter was used to generate a sinusoidal 1 Hz single frequency EIS signal at 10 mV_{rms} with 0 V_{dc} offset. The resulting current at the working electrode of the sensor was measured using a low-side current sense circuit. The resulting response was captured and compared to the excitation signal to calculate the effective impedance over the sensor. An analog-to-digital converter to read results back to the microcontroller for reporting. For this first-generation device, analysis was done off-board post data acquisition.

Results and Discussion

ATR-FTIR characterization

Figure 19a shows the ATR-FTIR spectra for the binding of the EDC-NHS complex to the molybdenum electrode interface, as well as the binding of IL-6 and CRP antibody to the bound EDC-NHS complex. The first measurement was done on a bare molybdenum surface pre-functionalization steps. The spectrum shows an absence of discernible peaks with a broad peak manifesting from 900 – 1100 cm^{-1}. This broad peak is characteristic of the Mo-O oxide layer that is leveraged for EDC-NHS binding. The oxide peak is still present, but less noticeable in the following functionalization steps as those measurements subtract the bare molybdenum baseline

from their measurement spectra. The peaks seen at 1649, 1645 cm^{-1}, and 1614 cm^{-1} are indicative of the v(C=O) carbonyl stretching of the EDC-NHS, but will be visible even after antibody conjugation to the EDC-NHS. The peak at 1564 cm^{-1} is characteristic of the N-H stretch of the EDC. The peaks at 1262, 1254, and 1267 cm^{-1} are from v(C-N) vibrational stretching also seen in all three measurements. The 1229 cm^{-1} peak in the EDC-NHS spectrum is from the stretching vibration of the v(N-O) as part of the NHS group and is not visible in either of the antibody measurements which is indicative of antibody binding to the EDC-NHS. These results give evidence that the EDC-NHS complex is binding to the oxide layer of the molybdenum surface, and that both the IL-6 and CRP antibodies are subsequently binding to the EDC-NHS.

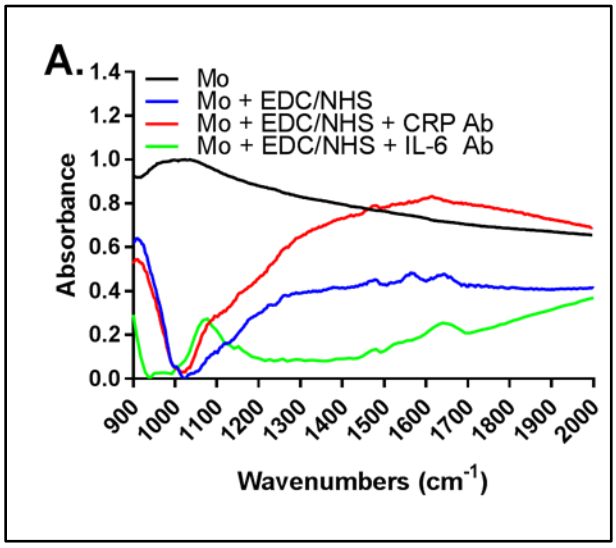

Figure 19. FTIR spectra of antibody binding on crosslinker functionalized Mo surface

ATR-FTIR spectra of bare molybdenum electrode, EDC-NHS functionalized electrode, Functionalized electrodes with CRP Antibody, and functionalized electrodes with IL-6 Antibody. The functionalization spectra have the bare Mo spectra subtracted out

Electrochemical detection of CRP and IL-6 in synthetic urine

Electrochemical detection of CRP and IL-6 were demonstrated in synthetic urine in three pH ranges namely pH 5.5, 6.5 and 7.5. The biosensor's impedance response was evaluated by calculating the percentage change in the modulus of impedance post the antibody functionalization step. Figure 20A shows the EIS characterization of CRP antigen concentrations in synthetic urine. A low CRP antigen concentration of 1 pg/mL and a high CRP concentration of 100 ng/mL was tested for three pH ranges namely 5.5, 6.5 and 7.5. Figure 20A shows the change in impedance with respect to the baseline functionalization step for low and high CRP antigen concentrations. The impedance values were analyzed at 1 Hz frequency. The analysis frequency was determined from the Bode phase analysis which is explained in Appendix. The sensor demonstrated same trend in impedance for all three pH buffer ranges of synthetic urine. Figure 20B shows the change in impedance for pH buffer 6.45. The change in impedance ranged approximately 20% for 1 pg/ml CRP concentration to 60 % for 100 ng/ml CRP concentration. A specific signal threshold (SST) of 13% was calculated for the CRP detection assay steps with a signal to noise ratio of 3. Figure 20C represents the percentage change in impedance for the low and high IL-6 antigen concentrations. An increasing trend in modulus of change in impedance was observed for increasing IL-6 antigen concentrations. This trend was observed in all three pH ranges. The change in impedance is the result of capacitive binding between the IL-6 antibody and IL-6 antigen. The percentage change in impedance for 1 pg/ml of IL-6 antigen with respect to the baseline functionalization step was calculated to be approximately 20 % for all three pH ranges which was above the measured an SST of 11 % calculated with a signal to noise ratio of 3. A change in impedance of approximately 50% was measured for the high concentration of 10 ng/mL (Figure

20D). The biomolecular binding at the electrode electrolyte interfaces increases the double layer capacitance resulting in the change in impedance.

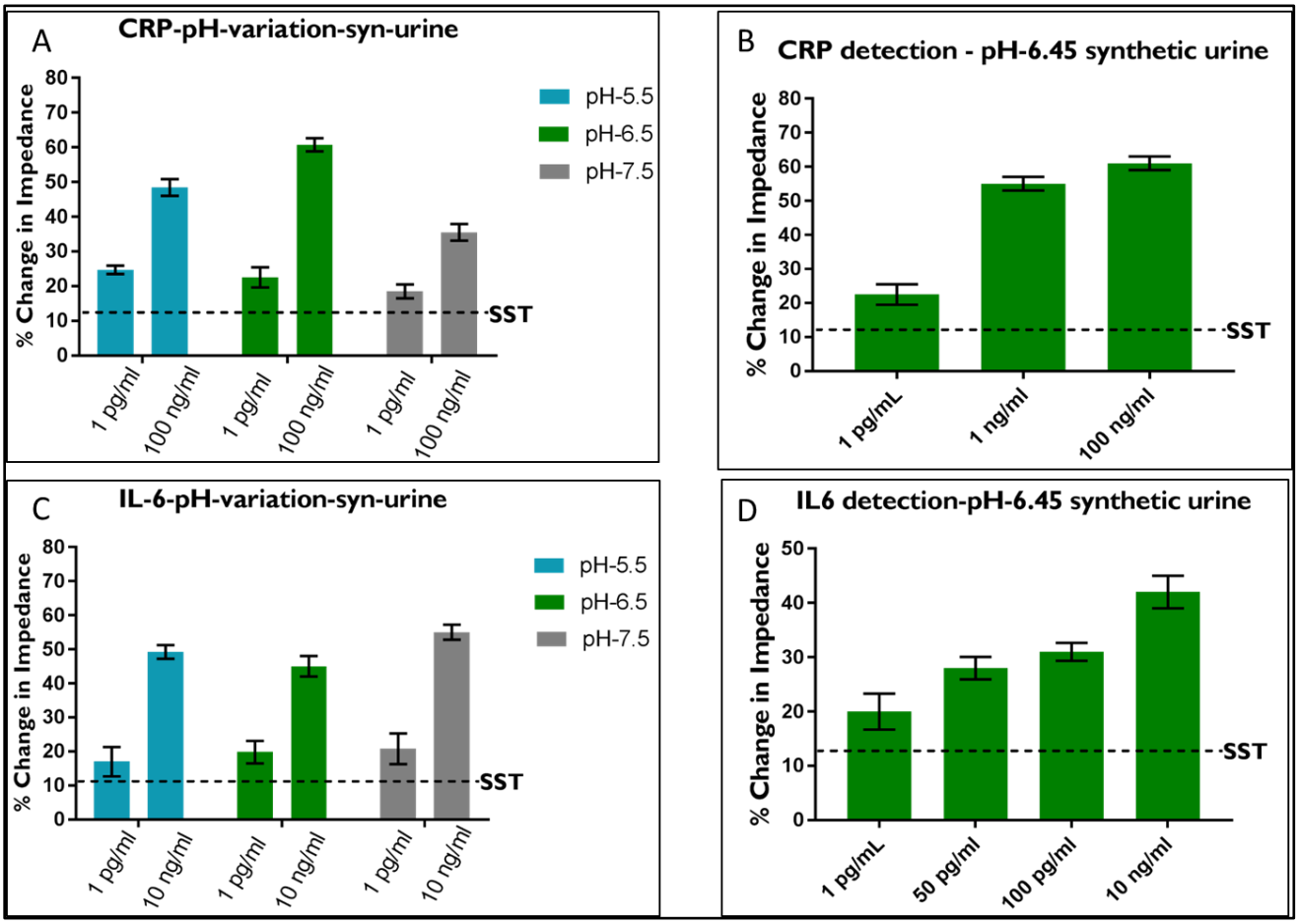

Figure 20. Detection of CRP and IL-6 in synthetic urine with varying pH

(**A**) Change in impedance analysis for low and high CRP antigen concentrations in three pH ranges of synthetic urine. Dotted lines indicate specific signal threshold (SST) (**B**) Impedance analysis for pH 6.45 synthetic urine. (**C**) Change in impedance analysis for low and high IL-6 antigen concentrations in three pH buffer ranges of synthetic urine. The dotted lines indicate Specific Signal Threshold. (**D**) Change in impedance analysis for four IL-6 antigen concentrations in pH 6.5 buffer of synthetic urine.

Electrochemical detection of CRP and IL-6 in human urine

The detection of CRP and IL-6 antigen concentrations were performed in pooled human urine samples. The mean pH of the human urine samples were measured to be 6.4.

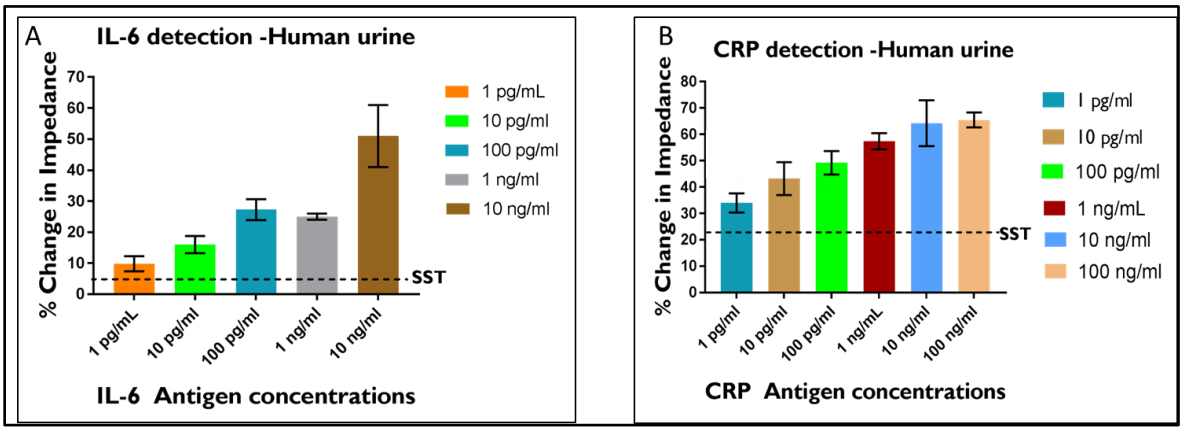

Figure 21. Dose response analysis for CRP and IL-6 detection in human urine

(A) Change in impedance analysis for CRP antigen concentrations (B) Change in impedance analysis for IL-6 antigen concentrations. Dotted lines indicate specific signal threshold (SST)

Figure 21A indicates the change in impedance for increasing CRP antigen concentrations from 1 pg/mL to 100 ng/mL. An SST of 21 % was calculated for the CRP detection assay. The limit of detection was therefore determined to be at 1 pg/mL. The change in impedance varied from 30 % to 61 % between the lowest and highest antigen concentrations. Figure 21B shows the change in impedance for the IL-6 antigen concentrations. The LoD for the IL-6 assay was also determined to be 1 pg/mL. The change in impedance for the highest IL-6 concentration of 10 ng/mL was measured to be approximately 50%.

Thus, clear distinguishability in impedance curves were obtained for both CRP and IL-6 biomolecules. The change in impedances were the result of capacitive changes occurring due to

biomolecular binding at the molybdenum electrode surface. The detection of both the inflammatory biomarkers is favored for specific disease detection and prognosis.

Comparison of impedance response with portable electronic hardware prototype

To demonstrate the translatability of the developed multiplexed dipstick assay into a true portable and PoC device, a portable reader was created for single frequency EIS analysis of the sensor at the 1 Hz point of analysis used for detection of the target proteins on the benchtop instrument. The device was designed to capture the changes in impedance response of the sensor from the post-functionalization baseline to the selected dose regimes of either CRP or IL-6 to the same level of sensitivity as can be attained by the benchtop instrument. For this proof-of-concept device LED indicators were used to report the detected levels of target protein (blank/no detection, 1 – 100 pg/mL, and 100 ng/mL). This correlation is plotted in figure 22 and shows a linear response with an R^2 value of 0.99. The governing equation $y = 1.058x – 141.6$ shows a near 1 slope. A 141.6 Ω offset exists between the two instruments, but the offset is constant and predictable between measurements making it easily accounted for. The main source of error in the correlation of the two tools came from fluctuations in solution resistance as function of time when reconfiguring the sensor from one tool to another, which is not a factor of the device itself. Overall, the device demonstrates translatability of the urine dipstick for inflammatory biomarkers towards a true PoC diagnostic form factor.

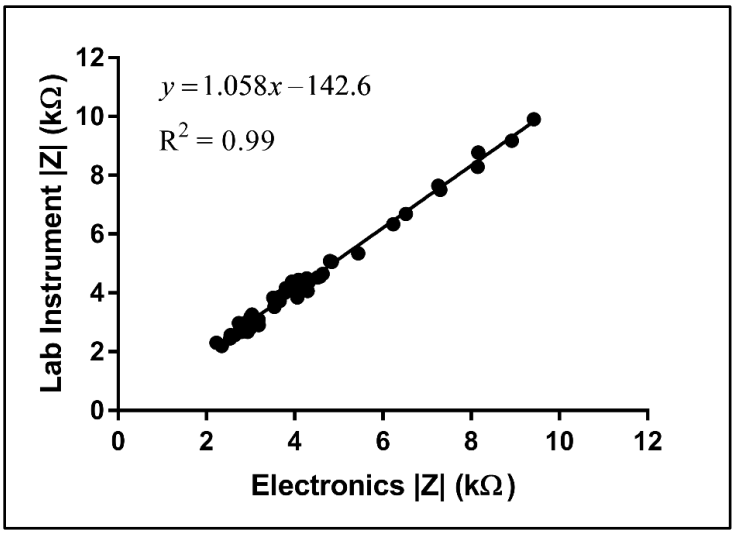

Figure 22. Linear impedance correlation between electronic device and lab instrument.

Conclusions

An affinity based electrochemical biosensor for the detection of two critical inflammatory biomarkers namely CRP and IL-6 was developed using Mo electrode. Binding characteristics of CRP and IL-6 antibody with EDC-NHS functionalized Mo surface was validated using FTIR technique. The affinity based antigen-antibody binding was characterized through non-faradaic electrochemical impedance spectroscopy. The biosensor exhibited ability to detect CRP and IL-6 antigen concentration as low as 1 pg/ml in both pooled human urine and synthetic urine samples. The sensor demonstrated stability in performance in multiple pH buffer ranges.

CHAPTER 7

CONCLUSION

In this dissertation, molybdenum (Mo) has been evaluated as an electrode material for affinity based electrochemical dipstick biosensor. The objective of this work is to develop a stable electrode system for reliable detection of target biomolecules using affinity based electrochemical dipstick biosensors. A stable deposition profile was observed for multiple fabrication batches. The biosensing application of Mo electrode was demonstrated through the detection of inflammatory biomarkers namely CRP and IL-6.

The deposition parameters for electron beam evaporation based Mo electrode on a porous flexible polyamide substrate were defined and the deposition profile of the fabricated sensor was evaluated through material characterization techniques such as SEM and EDAX. These results are discussed in chapter 2. The preliminary evaluation of affinity based biosensing application was performed using cTnI biomolecule.

In chapter 3, the interaction between Mo electrode surface and the crosslinker molecules were investigated. Two crosslinker molecules namely DSP and EDC-NHS were evaluated and the binding affinity between the crosslinker molecules with Mo electrode was characterized using FTIR, XPS and fluorescence microscopy characterization methods. Electrochemical characterization of the Mo electrode in varied buffers were characterized.

In chapter 4, affinity based electrochemical biosensing application was demonstrated with Mo electrode was performed using non-faradaic electrochemical impedance spectroscopy technique.

In chapter 5, the chemical affinity between Mo with thiol and carbodiimide crosslinkers were

investigated using FTIR, XPS, fluorescence microscopy and contact angle measurements. In chapter 6, electrochemical affinity based urine dipstick detection was discussed. Two inflammatory biomarkers namely CRP and IL-6 were detected in the range from 1 pg/ml to 100 ng/mL for CRP and from 1 pg/ml to 10 ng/mL for IL-6. The detection of these biomarkers were tested in human urine and synthetic urine samples in multiple pH ranges. The sensor performance was tested using a standard benchtop commercial potentiostat and a portable electronic potentiostat.

Thus, Mo displayed favorable electrochemical properties for use as an electrode material. The surface morphology analysis indicated the possibility of achieving a uniform electrode deposition. The surface characterization analysis proved the presence of chemical affinity between the crosslinker molecules with Mo electrode. The electrode established the ability to detect change in impedance between varying assay conditions and hence holds scope for use as electrode material in affinity based electrochemical biosensors.

APPENDIX

Nyquist and Bode Phase analysis for CRP and IL-6 detection

The frequency response study of the biosensor for the detection of IL-6 and CRP was performed with Bode phase and Nyquist plots. The frequency of the input voltage signal was swept from 0.1 Hz to 1 MHz. Figure 23 demonstrates the Nyquist and Bode phase plots for IL-6 and CRP detection in synthetic urine buffer with pH 6.5.

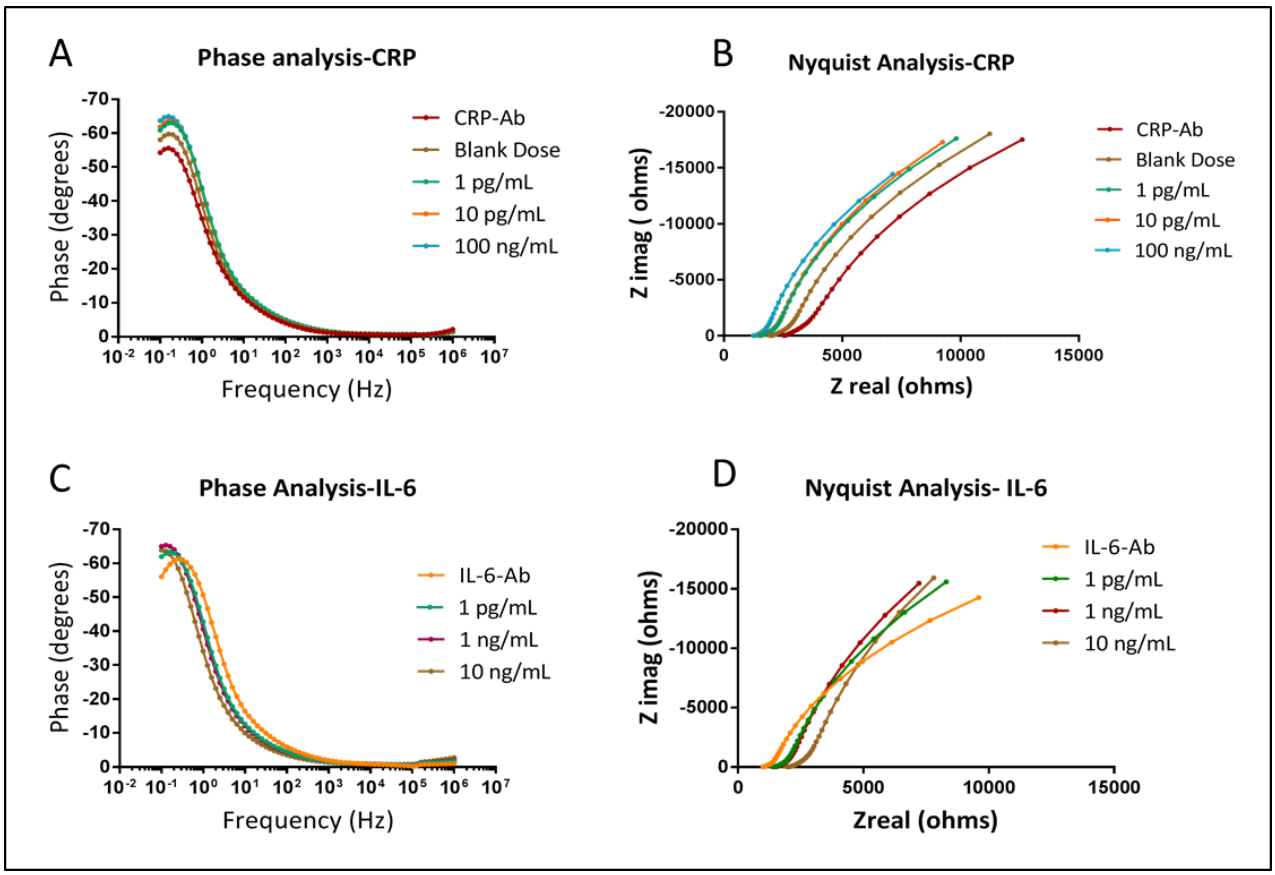

Figure 23. Nyquist and Bode Phase analysis for IL-6 and CRP detection

A. Phase analysis of CRP indicates the presence of dominant capacitive reactance at 1 Hz frequency. **B.** Nyquist plot indicates the correlation between CRP antigen concentration and impedance values. **C.** Phase response indicates the presence of capacitive reactance at 1 Hz

frequency. **D.** Nyquist plot indicates the correlation between the IL-6 antigen and impedance values.

The Bode phase plot of CRP (Figure 23A) indicates the change in phase of the impedance with frequencies. The phase plot demonstrated a capacitive reactance region at 1 Hz where a dominant capacitance and resistance component was present. Thus, this transition frequency was selected for impedance analysis for subsequent assay steps. Similarly, Bode phase plot of IL-6 (Figure 23 C) also demonstrated a capacitive reactance region at 1 Hz. Figure 23B shows the Nyquist response for varying CRP antigen concentrations. Nyquist plot demonstrated a correlation between CRP concentrations and impedance values. Similarly, the Nyquist plot for IL-6 detection (Figure 23D) also demonstrated a trend in the impedance values which is correlated with concentration of the IL-6 antigen. The shift in the x intercept of the Nyquist plot is explained as the variation in the solution resistance component (R_{sol}). The change in the solution resistance is attributed to the bulk ionic effect resulting from the constituents of the buffer solution. Thus, the Nyquist response of CRP and IL-6 assays demonstrated the ability to detect the change in impedance for multiple assay steps and establish a correlation with the antigen concentration.

REFERENCES

1.Baryeh, K.; Takalkar, S.; Lund, M.; Liu, G., 1 - Introduction to medical biosensors for point of care applications A2 - Narayan, Roger J. In *Medical Biosensors for Point of Care (POC) Applications*, Woodhead Publishing: 2017; pp 3-25.

2.Daniels, J. S.; Pourmand, N., Label-free impedance biosensors: Opportunities and challenges. *Electroanalysis* **2007,** *19* (12), 1239-1257.

3.Gubala, V.; Harris, L. F.; Ricco, A. J.; Tan, M. X.; Williams, D. E., Point of Care Diagnostics: Status and Future. *Analytical Chemistry* **2012,** *84* (2), 487-515.

4.Kim, J.-Y.; Jang, D.; Greer, J. R., Tensile and compressive behavior of tungsten, molybdenum, tantalum and niobium at the nanoscale. *Acta Materialia* **2010,** *58* (7), 2355-2363.

5. Saji, V. S.; Lee, C. W., Molybdenum, molybdenum oxides, and their electrochemistry. *ChemSusChem* **2012,** *5* (7), 1146-1161.

6.Cherng, J.; Chen, T.; Lin, C., Pulsed-DC sputtering of molybdenum bottom electrode and piezoelectric aluminum nitride films for bulk acoustic resonator applications. *Thin Solid Films* **2011,** *519* (20), 6797-6800.

7.Cao, Q.; Hur, S. H.; Zhu, Z. T.; Sun, Y. G.; Wang, C. J.; Meitl, M. A.; Shim, M.; Rogers, J. A., Highly Bendable, Transparent Thin-Film Transistors That Use Carbon-Nanotube-Based Conductors and Semiconductors with Elastomeric Dielectrics. *Advanced Materials* **2006,** *18* (3), 304-309.

8. Padilha, J. C.; Martini, E. M. A.; Brum, C.; de Souza, M. O.; de Souza, R. F., Study of molybdenum electrodes for hydrogen evolution reaction. *Journal of Power Sources* **2009,** *194* (1), 482-485.

9.Gao, M.-R.; Liang, J.-X.; Zheng, Y.-R.; Xu, Y.-F.; Jiang, J.; Gao, Q.; Li, J.; Yu, S.-H., An efficient molybdenum disulfide/cobalt diselenide hybrid catalyst for electrochemical hydrogen generation. *Nature communications* **2015,** *6*.

10.Cheng, R.; Jiang, S.; Chen, Y.; Liu, Y.; Weiss, N.; Cheng, H.-C.; Wu, H.; Huang, Y.; Duan, X., Few-layer molybdenum disulfide transistors and circuits for high-speed flexible electronics. **2014,** *5*, 5143.

11.Shen, B.; Malshe, A. P.; Kalita, P.; Shih, A. J., Performance of novel MoS2 nanoparticles based grinding fluids in minimum quantity lubrication grinding. *Trans. NAMRI/SME* **2008,** *36* (357), e364.

12.(a) Wu, H. B.; Xia, B. Y.; Yu, L.; Yu, X.-Y.; Lou, X. W. D., Porous molybdenum carbide nano-octahedrons synthesized via confined carburization in metal-organic frameworks for efficient hydrogen production. *Nature communications* **2015,** *6*; (b) Wu, M.; Lin, X.; Hagfeldt, A.; Ma, T., Low-Cost Molybdenum Carbide and Tungsten Carbide Counter Electrodes for Dye-Sensitized Solar Cells. *Angewandte Chemie International Edition* **2011,** *50* (15), 3520-3524.

13.Ghosh, R. N.; Askeland, P. A.; Kramer, S.; Loloee, R., Optical dissolved oxygen sensor utilizing molybdenum chloride cluster phosphorescence. *Applied Physics Letters* **2011,** *98* (22), 221103.

14.(a) Sarkar, D.; Liu, W.; Xie, X.; Anselmo, A. C.; Mitragotri, S.; Banerjee, K., MoS2 Field-Effect Transistor for Next-Generation Label-Free Biosensors. *ACS Nano* **2014,** *8* (4), 3992-4003; (b) Lee, J.; Dak, P.; Lee, Y.; Park, H.; Choi, W.; Alam, M. A.; Kim, S., Two-dimensional layered MoS2 biosensors enable highly sensitive detection of biomolecules. *Scientific reports* **2014,** *4*.

15.Hille, R.; Hall, J.; Basu, P., The Mononuclear Molybdenum Enzymes. *Chemical Reviews* **2014,** *114* (7), 3963-4038.

16. (a) Li, Z.-H.; Cho, E.-S.; Kwon, S. J., Molybdenum thin film deposited by in-line DC magnetron sputtering as a back contact for Cu(In,Ga)Se2 solar cells. *Applied Surface Science* **2011,** *257* (22), 9682-9688; (b) Pethe, S. A.; Takahashi, E.; Kaul, A.; Dhere, N. G., Effect of sputtering process parameters on film properties of molybdenum back contact. *Solar Energy Materials and Solar Cells* **2012,** *100*, 1-5.

17.Khan, M.; Islam, M., Deposition and characterization of molybdenum thin films using dc-plasma magnetron sputtering. *Semiconductors* **2013,** *47* (12), 1610-1615.

18.https://pubchem.ncbi.nlm.nih.gov/compound/23932.

19.Vink, T. J.; Somers, M. A. J.; Daams, J. L. C.; Dirks, A. G., Stress, strain, and microstructure of sputter-deposited Mo thin films. *Journal of Applied Physics* **1991,** *70* (8), 4301-4308.

20.Zhang, S.; Wang, N.; Yu, H.; Niu, Y.; Sun, C., Covalent attachment of glucose oxidase to an Au electrode modified with gold nanoparticles for use as glucose biosensor. *Bioelectrochemistry* **2005,** *67* (1), 15-22.

21.Farsinezhad, S.; Mohammadpour, A.; Dalrymple, A. N.; Geisinger, J.; Kar, P.; Brett, M. J.; Shankar, K., Transparent anodic TiO2 nanotube arrays on plastic substrates for disposable biosensors and flexible electronics. *Journal of nanoscience and nanotechnology* **2013,** *13* (4), 2885-2891.

22.Lue, C.-E.; Wang, I.-S.; Huang, C.-H.; Shiao, Y.-T.; Wang, H.-C.; Yang, C.-M.; Hsu, S.-H.; Chang, C.-Y.; Wang, W.; Lai, C.-S., pH sensing reliability of flexible ITO/PET electrodes on EGFETs prepared by a roll-to-roll process. *Microelectronics Reliability* **2012,** *52* (8), 1651-1654.

23.(a) Arecchi, A.; Scampicchio, M.; Drusch, S.; Mannino, S., Nanofibrous membrane based tyrosinase-biosensor for the detection of phenolic compounds. *Analytica Chimica Acta* **2010,** *659* (1), 133-136; (b) Scampicchio, M.; Arecchi, A.; Lawrence, N. S.; Mannino, S., Nylon nanofibrous membrane for mediated glucose biosensing. *Sensors and Actuators B: Chemical* **2010,** *145* (1), 394-397.

24.Panneer Selvam, A.; Prasad, S.; Barrett, T. W.; Kazmierczak, S. C., Electrical nanowell diagnostics sensors for rapid and ultrasensitive detection of prostate-specific antigen. *Nanomedicine* **2015,** *10* (16), 2527-2536.

25.Rogers, K. R., Principles of affinity-based biosensors. *Molecular Biotechnology* **2000,** *14* (2), 109-129.

26.Selvam, A. P.; Prasad, S., Nanosensor electrical immunoassay for quantitative detection of NT-pro brain natriuretic peptide. *Future cardiology* **2013,** *9* (1), 137-147.

27.Prasad, S.; Tyagi, A. K.; Aggarwal, B. B., Detection of inflammatory biomarkers in saliva and urine: Potential in diagnosis, prevention, and treatment for chronic diseases. *Experimental Biology and Medicine* **2016,** *241* (8), 783-799.

28.El-Khier, N. A.; Ael, R. E. G.; Elgeidy, A.; Rakha, S. A., Assessment of interleukin-6 and other inflammatory markers in the diagnosis of Egyptian patients with periprosthetic joint infection. *Egypt J Immunol* **2013,** *20*, 93-99.

29.Chou, S.-C.; Ko, H.-W.; Lin, Y.-C., CRP/IL-6/IL-10 Single-Nucleotide Polymorphisms Correlate with the Susceptibility and Severity of Community-Acquired Pneumonia. *Genetic Testing and Molecular Biomarkers* **2016,** *20* (12), 732-740.

30.Paik, J. K.; Kim, O. Y.; Koh, S. J.; Jang, Y.; Chae, J. S.; Kim, J. Y.; Kim, H. J.; Hyun, Y. J.; Cho, J. R.; Lee, J. H., Additive effect of interleukin-6 and C-reactive protein (CRP) single nucleotide polymorphism on serum CRP concentration and other cardiovascular risk factors. *Clinica Chimica Acta* **2007,** *380* (1), 68-74.

31.Filik, L.; Dagli, U.; Ulker, A., C-reactive protein and monitoring the activity of Crohn's disease. *Advances in Therapy* **2006,** *23* (4), 655-662.

32.Liang, K. Z.; Mu, W. J., Flow-injection immuno-bioassay for interleukin-6 in humans based on gold nanoparticles modified screen-printed graphite electrodes. *Analytica Chimica Acta* **2006,** *580* (2), 128-135.

33.Wang, S.; Chinnasamy, T.; Lifson, M. A.; Inci, F.; Demirci, U., Flexible Substrate-Based Devices for Point-of-Care Diagnostics. *Trends in Biotechnology*.

34.Hu, J.; Wang, S.; Wang, L.; Li, F.; Pingguan-Murphy, B.; Lu, T. J.; Xu, F., Advances in paper-based point-of-care diagnostics. *Biosensors and Bioelectronics* **2014,** *54*, 585-597.

35.(a) Wan, Y.; Su, Y.; Zhu, X.; Liu, G.; Fan, C., Development of electrochemical immunosensors towards point of care diagnostics. *Biosensors and Bioelectronics* **2013,** *47*, 1-11; (b) Panpradist, N.; Lai, J. J., 4.1 - Point-of-Care Diagnostics A2 - Ebara, Mitsuhiro. In *Biomaterials Nanoarchitectonics*, William Andrew Publishing: 2016; pp 139-156.

36.Zhou, J.; Gan, N.; Hu, F.; Li, T.; Zhou, H.; Li, X.; Zheng, L., A single antibody sandwich electrochemiluminescence immunosensor based on protein magnetic molecularly imprinted polymers mimicking capture probes. *Sensors and Actuators B: Chemical* **2013,** *186*, 300-307.

37.Carminati, M.; Vergani, M.; Ferrari, G.; Caranzi, L.; Caironi, M.; Sampietro, M., Accuracy and resolution limits in quartz and silicon substrates with microelectrodes for electrochemical biosensors. *Sensors and Actuators B: Chemical* **2012,** *174*, 168-175.

38.(a) Shafiee, H.; Asghar, W.; Inci, F.; Yuksekkaya, M.; Jahangir, M.; Zhang, M. H.; Durmus, N. G.; Gurkan, U. A.; Kuritzkes, D. R.; Demirci, U., Paper and Flexible Substrates as Materials for Biosensing Platforms to Detect Multiple Biotargets. *Scientific Reports* **2015,** *5*, 8719; (b) Martinez, A. W.; Phillips, S. T.; Whitesides, G. M.; Carrilho, E., Diagnostics for the Developing World: Microfluidic Paper-Based Analytical Devices. *Analytical Chemistry* **2010,** *82* (1), 3-10.

39. (a) Cui, G.; Kim, S. J.; Choi, S. H.; Nam, H.; Cha, G. S.; Paeng, K.-J., A Disposable Amperometric Sensor Screen Printed on a Nitrocellulose Strip: A Glucose Biosensor Employing Lead Oxide as an Interference-Removing Agent. *Analytical Chemistry* **2000,** *72* (8), 1925-1929; (b) Nguyen, B. T. T.; Peh, A. E. K.; Chee, C. Y. L.; Fink, K.; Chow, V. T. K.; Ng, M. M. L.; Toh, C.-S., Electrochemical impedance spectroscopy characterization of nanoporous alumina dengue virus biosensor. *Bioelectrochemistry* **2012,** *88*, 15-21.

40.Adiga, S. P.; Jin, C.; Curtiss, L. A.; Monteiro-Riviere, N. A.; Narayan, R. J., Nanoporous membranes for medical and biological applications. *Wiley Interdisciplinary Reviews: Nanomedicine and Nanobiotechnology* **2009,** *1* (5), 568-581.

41.(a) Assolant-vinet, C. H.; Coulet, P. R., New Immobilized Enzyme Membranes for Tailor-Made Biosensors. *Analytical Letters* **1986,** *19* (7-8), 875-885; (b) Marquette, C. A.; Leca, B. D.; Blum, L. J., Electrogenerated chemiluminescence of luminol for oxidase-based fibre-optic biosensors. *Luminescence* **2001,** *16* (2), 159-165; (c) Munje, R. D.; Muthukumar, S.; Panneer Selvam, A.; Prasad, S., Flexible nanoporous tunable electrical double layer biosensors for sweat diagnostics. *Scientific Reports* **2015,** *5*, 14586.

42.Uehara, H.; Kakiage, M.; Sekiya, M.; Sakuma, D.; Yamonobe, T.; Takano, N.; Barraud, A.; Meurville, E.; Ryser, P., Size-Selective Diffusion in Nanoporous but Flexible Membranes for Glucose Sensors. *ACS Nano* **2009,** *3* (4), 924-932.

43. VATTIPALLI, K.; FEIKERT, P.; BRANDIGAMPALA, S.; PRASAD, S., Study of nanoporous membranes with applications in the enhanced detection of cadiovascular biomarker proteins. *Nano Life* **2010,** *1* (03n04), 175-183.

44.Bogomolova, A.; Komarova, E.; Reber, K.; Gerasimov, T.; Yavuz, O.; Bhatt, S.; Aldissi, M., Challenges of Electrochemical Impedance Spectroscopy in Protein Biosensing. *Analytical Chemistry* **2009,** *81* (10), 3944-3949.

45.Kalantar-zadeh, K.; Ou, J. Z., Biosensors Based on Two-Dimensional MoS2. *ACS Sensors* **2016,** *1* (1), 5-16.

46.Mele, L.; Santagata, F.; Iervolino, E.; Mihailovic, M.; Rossi, T.; Tran, A. T.; Schellevis, H.; Creemer, J. F.; Sarro, P. M., A molybdenum MEMS microhotplate for high-temperature operation. *Sensors and Actuators A: Physical* **2012,** *188*, 173-180.

47.(a) Zou, Z.; Han, J.; Jang, A.; Bishop, P. L.; Ahn, C. H., A disposable on-chip phosphate sensor with planar cobalt microelectrodes on polymer substrate. *Biosensors and Bioelectronics* **2007,** *22* (9–10), 1902-1907; (b) Lang, X.-Y.; Fu, H.-Y.; Hou, C.; Han, G.-F.; Yang, P.; Liu, Y.-B.; Jiang, Q., Nanoporous gold supported cobalt oxide microelectrodes as high-performance electrochemical biosensors. *Nature communications* **2013,** *4*; (c) Patel, J.; Radhakrishnan, L.; Zhao, B.; Uppalapati, B.; Daniels, R. C.; Ward, K. R.; Collinson, M. M., Electrochemical Properties of Nanostructured Porous Gold Electrodes in Biofouling Solutions. *Analytical Chemistry* **2013,** *85* (23), 11610-11618.

48. Wang, D.-W.; Li, F.; Wu, Z.-S.; Ren, W.; Cheng, H.-M., Electrochemical interfacial capacitance in multilayer graphene sheets: Dependence on number of stacking layers. *Electrochemistry Communications* **2009,** *11* (9), 1729-1732.

49.Wikstrom, L.; Nobe, K., The Electrochemical Behavior of Molybdenum. *Journal of The Electrochemical Society* **1969,** *116* (4), 525-530.

50.Byskov, L. S.; Hammer, B.; Nørskov, J. K.; Clausen, B. S.; Topsøe, H., Sulfur bonding in MoS2 and Co-Mo-S structures. *Catalysis Letters* **1997,** *47* (3), 177-182.

51.(a) Cummins, B.; Auckland, M. L.; Cummins, P., Cardiac-specific troponin-l radioimmunoassay in the diagnosis of acute myocardial infarction. *American Heart Journal* **1987,** *113* (6), 1333-1344; (b) Bodor, G. S.; Porter, S.; Landt, Y.; Ladenson, J. H., Development of monoclonal antibodies for an assay of cardiac troponin-I and preliminary results in suspected cases of myocardial infarction. *Clinical Chemistry* **1992,** *38* (11), 2203-14.

52.Shen, W.; Tian, D.; Cui, H.; Yang, D.; Bian, Z., Nanoparticle-based electrochemiluminescence immunosensor with enhanced sensitivity for cardiac troponin I using N-(aminobutyl)-N-(ethylisoluminol)-functionalized gold nanoparticles as labels. *Biosensors and Bioelectronics* **2011,** *27* (1), 18-24.

53.Singal, S.; Srivastava, A. K.; Biradar, A. M.; Mulchandani, A.; Rajesh, Pt nanoparticles-chemical vapor deposited graphene composite based immunosensor for the detection of human cardiac troponin I. *Sensors and Actuators B: Chemical* **2014,** *205*, 363-370.

54.Qureshi, A.; Gurbuz, Y.; Niazi, J. H., Biosensors for cardiac biomarkers detection: A review. *Sensors and Actuators B: Chemical* **2012,** *171–172*, 62-76.

55.Dittmer, W. U.; Evers, T. H.; Hardeman, W. M.; Huijnen, W.; Kamps, R.; de Kievit, P.; Neijzen, J. H. M.; Nieuwenhuis, J. H.; Sijbers, M. J. J.; Dekkers, D. W. C.; Hefti, M. H.; Martens, M. F. W. C., Rapid, high sensitivity, point-of-care test for cardiac troponin based on optomagnetic biosensor. *Clinica Chimica Acta* **2010,** *411* (11–12), 868-873.

56.Wu, W.-Y.; Bian, Z.-P.; Wang, W.; Wang, W.; Zhu, J.-J., PDMS gold nanoparticle composite film-based silver enhanced colorimetric detection of cardiac troponin I. *Sensors and Actuators B: Chemical* **2010,** *147* (1), 298-303.

57.Kwon, Y.-C.; Kim, M.-G.; Kim, E.-M.; Shin, Y.-B.; Lee, S.-K.; Lee, S. D.; Cho, M.-J.; Ro, H.-S., Development of a surface plasmon resonance-based immunosensor for the rapid detection of cardiac troponin I. *Biotechnol Lett* **2011,** *33* (5), 921-927.

58.He, P.; Oncescu, V.; Lee, S.; Choi, I.; Erickson, D., Label-free electrochemical monitoring of vasopressin in aptamer-based microfluidic biosensors. *Analytica Chimica Acta* **2013,** *759*, 74-80.

59.Randviir, E. P.; Banks, C. E., Electrochemical impedance spectroscopy: an overview of bioanalytical applications. *Analytical Methods* **2013,** *5* (5), 1098-1115.

60.Luo, X.; Davis, J. J., Electrical biosensors and the label free detection of protein disease biomarkers. *Chemical Society Reviews* **2013,** *42* (13), 5944-5962.

61. Jacobs, M.; Muthukumar, S.; Panneer Selvam, A.; Engel Craven, J.; Prasad, S., Ultra-sensitive electrical immunoassay biosensors using nanotextured zinc oxide thin films on printed circuit board platforms. *Biosensors and Bioelectronics* **2014,** *55*, 7-13.

62.Lisdat, F.; Schäfer, D., The use of electrochemical impedance spectroscopy for biosensing. *Analytical and Bioanalytical Chemistry* **2008,** *391* (5), 1555-1567.

63.Saha, B.; Evers, T. H.; Prins, M. W. J., How Antibody Surface Coverage on Nanoparticles Determines the Activity and Kinetics of Antigen Capturing for Biosensing. *Analytical Chemistry* **2014,** *86* (16), 8158-8166.

64.(a) Yang, M.; Qu, F.; Lu, Y.; He, Y.; Shen, G.; Yu, R., Platinum nanowire nanoelectrode array for the fabrication of biosensors. *Biomaterials* **2006,** *27* (35), 5944-5950; (b) Liu, J.; Wang, J.; Wang, T.; Li, D.; Xi, F.; Wang, J.; Wang, E., Three-dimensional electrochemical immunosensor for sensitive detection of carcinoembryonic antigen based on monolithic and macroporous graphene foam. *Biosensors and Bioelectronics* **2015,** *65*, 281-286.

65.St John, A.; Price, C. P., Existing and emerging technologies for point-of-care testing. *The Clinical Biochemist Reviews* **2014,** *35* (3), 155.

66.Gonzalez-Macia, L.; Killard, A. J., 4 - Screen printing and other scalable point of care (POC) biosensor processing technologies A2 - Narayan, Roger J. In *Medical Biosensors for Point of Care (POC) Applications*, Woodhead Publishing: 2017; pp 69-98.

67.(a) Ahn, C. H.; Choi, J.-W.; Beaucage, G.; Nevin, J. H.; Lee, J.-B.; Puntambekar, A.; Lee, J. Y., Disposable smart lab on a chip for point-of-care clinical diagnostics. *Proceedings of the IEEE* **2004,** *92* (1), 154-173; (b) Jung, W.; Han, J.; Choi, J.-W.; Ahn, C. H., Point-of-care testing (POCT) diagnostic systems using microfluidic lab-on-a-chip technologies. *Microelectronic Engineering* **2015,** *132*, 46-57.

68.Muller, A.; Neculoiu, D.; Konstantinidis, G.; Stavrinidis, A.; Vasilache, D.; Cismaru, A.; Danila, M.; Dragoman, M.; Deligeorgis, G.; Tsagaraki, K., 6.3-GHz Film Bulk Acoustic Resonator Structures Based on a Gallium Nitride/Silicon Thin Membrane. *IEEE Electron Device Letters* **2009,** *30* (8), 799-801.

69.Smith, G. T.; Dwork, N.; Khan, S. A.; Millet, M.; Magar, K.; Javanmard, M.; Bowden, A. K. E., Robust dipstick urinalysis using a low-cost, micro-volume slipping manifold and mobile phone platform. *Lab on a Chip* **2016,** *16* (11), 2069-2078.

70.Chen, C.; Wu, Y.; Dong, T. In *Dipsticks integrated on smart diapers for colorimetric analysis of urinary tract infections in the field*, Mechatronics-Mechatronika (ME), 2014 16th International Conference on, IEEE: 2014; pp 423-427.

71.(a) Bertotti, M.; Pletcher, D., The reduction of bromate at molybdenum oxide film cathodes. *Electroanalysis* **1996,** *8* (12), 1105-1111; (b) Choi, J.-G.; Thompson, L., XPS study of as-prepared and reduced molybdenum oxides. *Applied Surface Science* **1996,** *93* (2), 143-149; (c) Liao, L.; Wang, S.; Xiao, J.; Bian, X.; Zhang, Y.; Scanlon, M. D.; Hu, X.; Tang, Y.; Liu, B.; Girault, H. H., A nanoporous molybdenum carbide nanowire as an electrocatalyst for hydrogen evolution reaction. *Energy & Environmental Science* **2014,** *7* (1), 387-392.

72.(a) Shon, J. K.; Lee, H. S.; Park, G. O.; Yoon, J.; Park, E.; Park, G. S.; Kong, S. S.; Jin, M.; Choi, J.-M.; Chang, H., Discovery of abnormal lithium-storage sites in molybdenum dioxide electrodes. *Nature communications* **2016,** *7*; (b) Park, D.-Y.; Sun, Y.-K.; Myung, S.-T., Carbothermal synthesis of molybdenum (IV) oxide as a high rate anode for rechargeable lithium batteries. *Journal of Power Sources* **2015,** *280*, 1-4.

73. Ivanov, A. B.; Volkovich, V. A.; Likhachev, P. Y.; Kamalov, R. V., Electrochemical Properties of Molybdenum in Alkali Chloride Melts. *ECS Transactions* **2014,** *64* (4), 377-387.

74.Badawy, W. A.; Al-Kharafi, F. M., Corrosion and passivation behaviors of molybdenum in aqueous solutions of different pH. *Electrochimica Acta* **1998,** *44* (4), 693-702.

75.Rodrigues, A. V.; Oliveira, N. T. C.; dos Santos, M. L.; Guastaldi, A. C., Electrochemical behavior and corrosion resistance of Ti–15Mo alloy in naturally-aerated solutions, containing chloride and fluoride ions. *Journal of Materials Science: Materials in Medicine* **2015,** *26* (1), 1.

76.Ribeiro, A. M.; Flores-Sahagun, T. H. S.; Paredes, R. C., A perspective on molybdenum biocompatibility and antimicrobial activity for applications in implants. *Journal of Materials Science* **2016,** *51* (6), 2806-2816.

77.Arora, K.; Chaubey, A.; Singhal, R.; Singh, R. P.; Pandey, M. K.; Samanta, S. B.; Malhotra, B. D.; Chand, S., Application of electrochemically prepared polypyrrole–polyvinyl sulphonate films to DNA biosensor. *Biosensors and Bioelectronics* **2006,** *21* (9), 1777-1783.

78.Barsan, M. M.; David, M.; Florescu, M.; Ţugulea, L.; Brett, C. M. A., A new self-assembled layer-by-layer glucose biosensor based on chitosan biopolymer entrapped enzyme with nitrogen doped graphene. *Bioelectrochemistry* **2014,** *99*, 46-52.

79. (a) Zhou, Y.; Zhi, J., Development of an amperometric biosensor based on covalent immobilization of tyrosinase on a boron-doped diamond electrode. *Electrochemistry Communications* **2006,** *8* (12), 1811-1816; (b) Sun, Y.; Wang, H.; Sun, C., Amperometric glucose biosensor based on layer-by-layer covalent attachment of AMWNTs and IO4−-oxidized GOx. *Biosensors and Bioelectronics* **2008,** *24* (1), 22-28.

80.(a) Timurdogan, E.; Alaca, B. E.; Kavakli, I. H.; Urey, H., MEMS biosensor for detection of Hepatitis A and C viruses in serum. *Biosensors and Bioelectronics* **2011,** *28* (1), 189-194; (b) Malsagova, K. A.; Ivanov, Y. D.; Pleshakova, T. O.; Kaysheva, A. L.; Shumov, I. D.; Kozlov, A. F.; Archakov, A. I.; Popov, V. P.; Fomin, B. I.; Latyshev, A. V., A SOI-nanowire biosensor for the multiple detection of D-NFATc1 protein in the serum. *Analytical Methods* **2015,** *7* (19), 8078-8085.

81.Arya, S. K.; Chornokur, G.; Venugopal, M.; Bhansali, S., Dithiobis(succinimidyl propionate) modified gold microarray electrode based electrochemical immunosensor for ultrasensitive detection of cortisol. *Biosensors and Bioelectronics* **2010,** *25* (10), 2296-2301.

82. (a) Arya, S. K.; Prusty, A. K.; Singh, S. P.; Solanki, P. R.; Pandey, M. K.; Datta, M.; Malhotra, B. D., Cholesterol biosensor based on N-(2-aminoethyl)-3-aminopropyl-trimethoxysilane self-assembled monolayer. *Analytical Biochemistry* **2007,** *363* (2), 210-218; (b) Hosseini, S.; Ibrahim, F.; Djordjevic, I.; Rothan, H. A.; Yusof, R.; van der Marel, C.; Benzina, A.; Koole, L. H., Synthesis and characterization of methacrylic microspheres for biomolecular recognition: Ultrasensitive biosensor for Dengue virus detection. *European Polymer Journal* **2014,** *60*, 14-21.

83. Ryckman, J. D.; Liscidini, M.; Sipe, J. E.; Weiss, S. M., Direct Imprinting of Porous Substrates: A Rapid and Low-Cost Approach for Patterning Porous Nanomaterials. *Nano Letters* **2011,** *11* (5), 1857-1862.

84.(a) Fichtlscherer, S.; Rosenberger, G.; Walter, D. H.; Breuer, S.; Dimmeler, S.; Zeiher, A. M., Elevated C-Reactive Protein Levels and Impaired Endothelial Vasoreactivity in Patients With Coronary Artery Disease. *Circulation* **2000,** *102* (9), 1000-1006; (b) Chuang, Y.-C.; Tyagi, V.;

Liu, R.-T.; Chancellor, M. B.; Tyagi, P., Urine and Serum C-Reactive Protein Levels as Potential Biomarkers of Lower Urinary Tract Symptoms. *Urological Science 21* (3), 132-136.

85.Chuang, Y.-C.; Tyagi, V.; Liu, R.-T.; Chancellor, M. B.; Tyagi, P., Urine and serum C-reactive protein levels as potential biomarkers of lower urinary tract symptoms. *Urological Science* **2010,** *21* (3), 132-136.

86.(a) Lessel, M.; Bäumchen, O.; Klos, M.; Hähl, H.; Fetzer, R.; Paulus, M.; Seemann, R.; Jacobs, K., Self-assembled silane monolayers: an efficient step-by-step recipe for high-quality, low energy surfaces. *Surface and Interface Analysis* **2015,** *47* (5), 557-564; (b) Borges, J.; Mano, J. F., Molecular Interactions Driving the Layer-by-Layer Assembly of Multilayers. *Chemical Reviews* **2014,** *114* (18), 8883-8942.

87.Maugé, F.; Lamotte, J.; Nesterenko, N.; Manoilova, O.; Tsyganenko, A., FT-IR study of surface properties of unsupported MoS 2. *Catalysis today* **2001,** *70* (1), 271-284.

88.Lacoste, J.; Carlsson, D. J., Gamma-, photo-, and thermally-initiated oxidation of linear low density polyethylene: A quantitative comparison of oxidation products. *Journal of Polymer Science Part A: Polymer Chemistry* **1992,** *30* (3), 493-500.

89. Rabolt, J.; Burns, F.; Schlotter, N.; Swalen, J., Anisotropic orientation in molecular monolayers by infrared spectroscopy. *The Journal of Chemical Physics* **1983,** *78* (2), 946-952.

90.Snoek, L. C.; Robertson, E. G.; Kroemer, R. T.; Simons, J. P., Conformational landscapes in amino acids: infrared and ultraviolet ion-dip spectroscopy of phenylalanine in the gas phase. *Chemical Physics Letters* **2000,** *321* (1–2), 49-56.

91. Mansur, H. S.; Sadahira, C. M.; Souza, A. N.; Mansur, A. A. P., FTIR spectroscopy characterization of poly (vinyl alcohol) hydrogel with different hydrolysis degree and chemically crosslinked with glutaraldehyde. *Materials Science and Engineering: C* **2008,** *28* (4), 539-548.

92.Schulz, H.; Baranska, M., Identification and quantification of valuable plant substances by IR and Raman spectroscopy. *Vibrational Spectroscopy* **2007,** *43* (1), 13-25.

93.Das, R. K.; Borthakur, B. B.; Bora, U., Green synthesis of gold nanoparticles using ethanolic leaf extract of Centella asiatica. *Materials Letters* **2010,** *64* (13), 1445-1447.

94.Son, D.; Chae, S. I.; Kim, M.; Choi, M. K.; Yang, J.; Park, K.; Kale, V. S.; Koo, J. H.; Choi, C.; Lee, M., Colloidal Synthesis of Uniform-Sized Molybdenum Disulfide Nanosheets for Wafer-Scale Flexible Nonvolatile Memory. *Advanced Materials* **2016,** *28* (42), 9326-9332.

95. Figueroa, C. A.; Ferlauto, A. S.; Alvarez, F., Identification of the mechanism-limiting nitrogen diffusion in metallic alloys by in situ photoemission electron spectroscopy. *Journal of Applied Physics* **2003,** *94* (8), 5435-5437.

96. (a) Thomsen, M.; Ingebrigtsen, T. S.; Marott, J. L.; Dahl, M.; Lange, P.; Vestbo, J.; Nordestgaard, B. G., Inflammatory biomarkers and exacerbations in chronic obstructive pulmonary disease. *Jama* **2013,** *309* (22), 2353-2361; (b) Zeng, F.; Wei, H.; Yeoh, E.; Zhang, Z.; Ren, Z.-F.; Colditz, G. A.; Tworoger, S. S.; Su, X., Inflammatory markers of CRP, IL-6, TNF-α and soluble TNFR2 and the risk of ovarian cancer: a meta-analysis of prospective studies. *Cancer Epidemiology Biomarkers & Prevention* **2016**; (c) Shlipak, M. G.; Fried, L. F.; Crump, C.; Bleyer, A. J.; Manolio, T. A.; Tracy, R. P.; Furberg, C. D.; Psaty, B. M., Elevations of Inflammatory and Procoagulant Biomarkers in Elderly Persons With Renal Insufficiency. *Circulation* **2003,** *107* (1), 87-92.

97.Van Oers, M.; Van der Heyden, A. A.; Aarden, L., Interleukin 6 (IL-6) in serum and urine of renal transplant recipients. *Clinical and experimental immunology* **1988,** *71* (2), 314.

98. Hedges, S.; Stenqvist, K.; Lidin-Janson, G.; Martinell, J.; Sandberg, T.; Svanborg, C., Comparison of Urine and Serum Concentrations of Interleukin-6 in Women with Acute Pyelonephritis or Asymtomatic Bacteriuria. *The Journal of Infectious Diseases* **1992,** *166* (3), 653-656.

99.Lafleur, J. P.; Jönsson, A.; Senkbeil, S.; Kutter, J. P., Recent advances in lab-on-a-chip for biosensing applications. *Biosensors and Bioelectronics* **2016,** *76*, 213-233.

100.(a) Link, N.; Weber, W.; Fussenegger, M., A novel generic dipstick-based technology for rapid and precise detection of tetracycline, streptogramin and macrolide antibiotics in food samples. *Journal of Biotechnology* **2007,** *128* (3), 668-680; (b) Selvakumar, L. S.; Thakur, M. S., Dipstick based immunochemiluminescence biosensor for the analysis of vitamin B12 in energy drinks: A novel approach. *Analytica Chimica Acta* **2012,** *722*, 107-113; (c) Vlachou, M. A.; Glynou, K. M.; Ioannou, P. C.; Christopoulos, T. K.; Vartholomatos, G., Development of a three-biosensor panel for the visual detection of thrombophilia-associated mutations. *Biosensors and Bioelectronics* **2010,** *26* (1), 228-234.

101. (a) Fernández-Sánchez, C.; McNeil, C. J.; Rawson, K.; Nilsson, O., Disposable Noncompetitive Immunosensor for Free and Total Prostate-Specific Antigen Based on Capacitance Measurement. *Analytical Chemistry* **2004,** *76* (19), 5649-5656; (b) Liang, M.; Fan, K.; Pan, Y.; Jiang, H.; Wang, F.; Yang, D.; Lu, D.; Feng, J.; Zhao, J.; Yang, L.; Yan, X., Fe3O4 Magnetic Nanoparticle Peroxidase Mimetic-Based Colorimetric Assay for the Rapid Detection of Organophosphorus Pesticide and Nerve Agent. *Analytical Chemistry* **2013,** *85* (1), 308-312.

102. Nemiroski, A.; Christodouleas, D. C.; Hennek, J. W.; Kumar, A. A.; Maxwell, E. J.; Fernández-Abedul, M. T.; Whitesides, G. M., Universal mobile electrochemical detector designed for use in resource-limited applications. *Proceedings of the National Academy of Sciences* **2014,** *111* (33), 11984-11989.

103. Su, L.; Feng, J.; Zhou, X.; Ren, C.; Li, H.; Chen, X., Colorimetric Detection of Urine Glucose Based ZnFe2O4 Magnetic Nanoparticles. *Analytical Chemistry* **2012,** *84* (13), 5753-5758.

104.Zangheri, M.; Di Nardo, F.; Mirasoli, M.; Anfossi, L.; Nascetti, A.; Caputo, D.; De Cesare, G.; Guardigli, M.; Baggiani, C.; Roda, A., Chemiluminescence lateral flow immunoassay cartridge with integrated amorphous silicon photosensors array for human serum albumin detection in urine samples. *Analytical and Bioanalytical Chemistry* **2016,** *408* (30), 8869-8879.

105.Soh, J. H.; Lin, Y.; Rana, S.; Ying, J. Y.; Stevens, M. M., Colorimetric Detection of Small Molecules in Complex Matrixes via Target-Mediated Growth of Aptamer-Functionalized Gold Nanoparticles. *Analytical Chemistry* **2015,** *87* (15), 7644-7652.

106.González-Guerrero, A. B.; Maldonado, J.; Dante, S.; Grajales, D.; Lechuga, L. M., Direct and label-free detection of the human growth hormone in urine by an ultrasensitive bimodal waveguide biosensor. *Journal of Biophotonics* **2017,** *10* (1), 61-67.

107.Diouf, A.; Motia, S.; Hassani, N. E. A. E.; Bari, N. E.; Bouchikhi, B. In *An electrochemical biosensor based on moleculary imprinted polymer for the quantification of creatinine in human urine samples*, 2017 ISOCS/IEEE International Symposium on Olfaction and Electronic Nose (ISOEN), 28-31 May 2017; 2017; pp 1-3.

108.Mach, K. E.; Mohan, R.; Patel, S.; Wong, P. K.; Hsieh, M.; Liao, J. C., Development of a Biosensor-Based Rapid Urine Test for Detection of Urogenital Schistosomiasis. *PLOS Neglected Tropical Diseases* **2015,** *9* (7), e0003845.

109. Li, N.; Wang, Y.; Li, Y.; Cao, W.; Ma, H.; Wu, D.; Du, B.; Wei, Q., A label-free electrochemical immunosensor based on Au@Pd/Ag yolk-bimetallic shell nanoparticles and amination graphene for detection of nuclear matrix protein 22. *Sensors and Actuators B: Chemical* **2014,** *202*, 67-73.

110.Xuan Viet, N.; Chikae, M.; Ukita, Y.; Maehashi, K.; Matsumoto, K.; Tamiya, E.; Hung Viet, P.; Takamura, Y., Gold-linked electrochemical immunoassay on single-walled carbon nanotube for highly sensitive detection of human chorionic gonadotropinhormone. *Biosensors and Bioelectronics* **2013,** *42*, 592-597.

111. Sánchez-Tirado, E.; Martínez-García, G.; González-Cortés, A.; Yáñez-Sedeño, P.; Pingarrón, J. M., Electrochemical immunosensor for sensitive determination of transforming growth factor (TGF) - β1 in urine. *Biosensors and Bioelectronics* **2017,** *88*, 9-14.

112.Smith, J. T.; Katchman, B. A.; Lee, Y. K.; Brien, B. P. O.; Bawolek, E. J.; Shah, S. S.; Christen, J. B. In *Disposable point-of-use optical biosensor for multiple biomarker detection*, 2014 IEEE Biomedical Circuits and Systems Conference (BioCAS) Proceedings, 22-24 Oct. 2014; 2014; pp 268-271.

113. Anilkumar, K. R.; Parveen, A.; Badiger, G. R.; Ambika Prasad, M. V. N., Effect of molybdenum trioxide (MoO3) on the electrical conductivity of polyaniline. *Physica B: Condensed Matter* **2009,** *404* (12–13), 1664-1667.

114. Kumagai, N.; Kumagai, N.; Tanno, K., Electrochemical characteristics and structural changes of molybdenum trioxide hydrates as cathode materials for lithium batteries. *Journal of Applied Electrochemistry* **1988,** *18* (6), 857-862.

115.Liu, C.; Li, Z.; Zhang, Z., Molybdenum oxide film with stable pseudocapacitive property for aqueous micro-scale electrochemical capacitor. *Electrochimica Acta* **2014,** *134*, 84-91.

116.Kim, H.-S.; Cook, J. B.; Lin, H.; Ko, J. S.; Tolbert, S. H.; Ozolins, V.; Dunn, B., Oxygen vacancies enhance pseudocapacitive charge storage properties of MoO3-x. *Nat Mater* **2017,** *16* (4), 454-460.

117.Sen, U. K.; Mitra, S., Synthesis of Molybdenum Oxides and their Electrochemical Properties against Li. *Energy Procedia* **2014,** *54*, 740-747.

118.Weng, Y.; Hou, R.; Li, G.; Wang, J.; Huang, N.; Liu, H., Immobilization of bovine serum albumin on TiO2 film via chemisorption of H3PO4 interface and effects on platelets adhesion. *Applied Surface Science* **2007**.

BIOGRAPHICAL SKETCH

Vikramshankar Kamakoti received his Bachelor of Technology (B.Tech) in Electronics and Instrumentation Engineering from SASTRA University, India in 2010. He worked with TATA consultancy services Ltd (TCS) for two years as Assistant Systems Engineer. He received his MS in Electrical Engineering from The University of Texas at Dallas in 2014. He joined the Biomedical Microdevices and Nanotechnology Lab for his PhD degree in Biomedical Engineering under the supervision of Dr. Shalini Prasad. He has gained experience in cleanroom fabrication, several electrical & material characterization techniques and immunoassay characterization experimentation.

CURRICULUM VITAE

VIKRAMSHANKAR KAMAKOTI

EDUCATION:

PhD. Biomedical Engineering, University of Texas at Dallas August 2017

M.S Electrical Engineering, University of Texas at Dallas May 2014

B.Tech Electronics & Instrumentation Engg, SASTRA University, India May 2010

PUBLICATIONS:

- **Kamakoti Vikramshankar**, Anjan Panneer Selvam, Nandhinee Radha Shanmugam, Sriram Muthukumar, and Shalini Prasad. "Flexible Molybdenum Electrodes towards Designing Affinity Based Protein Biosensors." Biosensors 6, no. 3 (2016): 36.

- Valekunja, Rohini Bhat, **Vikramshankar Kamakoti**, Anitha Peter, Shamprasad Phadnis, Shalini Prasad, and Vinay J. Nagaraj. "The detection of papaya ringspot virus coat protein using an electrochemical immunosensor." Analytical Methods 8, no. 48 (2016): 8534-8541.

- Selvam, Anjan Panneer, Sriram Muthukumar, **Vikramshankar Kamakoti**, and Shalini Prasad. "A wearable biochemical sensor for monitoring alcohol consumption lifestyle through Ethyl glucuronide (EtG) detection in human sweat." Scientific reports 6 (2016).

TEACHING ASSISTANTSHIP EXPERIENCE:

BMEN 4320- Intermediate Electrical Systems (Fall 2016)

BMEN 3130- Engineering Physiology Laboratory (Spring 2017)

PROFESSIONAL EXPERIENCE:

Assistant Systems Engineer, TATA Consultancy Services Ltd. July 2010 –June 2012

•Identification and mitigation of Information Technology security risks